CELL-FREE APPROACHES TO PROMOTE ENDOGENOUS REPAIR AFTER TRAUMATIC BRAIN INJURY

by

MIN KYOUNG SUN

(Under the Direction of Lohitash Karumbaiah)

ABSTRACT

Severe traumatic brain injuries (sTBI) culminate in lifelong disabilities as a consequence of the significant brain tissue loss and neuronal dysfunction encountered. Clinical management of sTBI is focused heavily on rehabilitation therapy, and there are no approved treatments to help replace brain tissue and to restore lost function. Neuroprotective “bystander” immunomodulatory and neurotrophic factor signaling that is activated after sTBI is regulated by endogenous neural stem cells (NSCs). However, these effects are transient and often overwhelmed by the cytotoxic and pro-inflammatory microenvironment surrounding the lesion site. In this work, I explore the use of cell-free approaches to promote endogenous functional repair after sTBI. I hypothesized that cell-free approaches involving the use of NSC derived extracellular vesicles (EVs), and brain-mimetic chondroitin sulfate (CS) -based 3D scaffolds can be tailored to create a localized neuroprotective microenvironment that is capable of sustaining cellular and functional repair of brain tissue after sTBI. These strategies present a novel means of accelerating endogenous functional repair mechanisms and could lead to the development of clinically relevant therapeutic interventions for sTBI patients in the future.

INDEX WORDS: Traumatic brain injury, brain mimetic, chondroitin sulfate, cell-free therapy, regeneration, extracellular vesicles

CELL-FREE APPROACHES TO PROMOTE ENDOGENOUS REPAIR AFTER TRAUMATIC BRAIN INJURY

by

MIN KYOUNG SUN

BS, The University of Pittsburgh, 2016

A Dissertation Submitted to the Graduate Faculty of The University of Georgia in Partial Fulfillment of the Requirements for the Degree

DOCTOR OF PHILOSOPHY

ATHENS, GEORGIA

2021

CELL-FREE APPROACHES TO PROMOTE ENDOGENOUS REPAIR AFTER

TRAUMATIC BRAIN INJURY

by

MIN KYOUNG SUN

Major Professor:	Lohitash Karumbaiah
Committee:	Philip V. Holmes
	Peter A. Kner
	Puliyur S. Mohankumar

Electronic Version Approved:

Ron Walcott
Vice Provost for Graduate Education and Dean of the Graduate School
The University of Georgia
August 2021

DEDICATION

This dissertation is dedicated to my family, who have been supportive and understanding halfway across the globe. Mom, and dad, you are the perfect parents I could have ever asked for and the reason I could be strong and independent during this unprecedented time. I am lucky to have both my sisters in my life to share smiles and laughter.

I also dedicate this work to Roman Carey, and Jessica Carpenter, who dealt with my insanity throughout five years of graduate school. Shadow, Ollie, and Otto for being great support dogs. Love you all.

ACKNOWLEDGEMENTS

I would like to thank my advisor, Dr. Lohitash Karumbaiah, for his guidance and encouragement to grow not only as a scientist, but also as a person. I appreciate the box of tissues you kept in your drawer for my emotional days. I would also like to thank my wonderful committee members, Dr. Philip V. Holmes, Dr. Peter Kner, and Dr. Puliyur S. Mohankumar. Thank you for being approachable and offering your time to give constructive feedback on my projects, as well as my career path.

Finally, I would like to thank the best lab mates, Meghan Logun, Dr. Charles-Francois Latchoumane, and Chaitanya Tondepu. Without your help, I do not know how I could have completed my work. You are not only excellent coworkers, but more importantly, amazing friends. Thank you to my incredible undergraduate students. I enjoyed working with you all.

TABLE OF CONTENTS

Page

LIST OF FIGURES

Page

CHAPTER 1

INTRODUCTION AND LITERATURE REVIEW

Severe traumatic brain injuries (sTBI) constitute a major health and socioeconomic problem due to its high mortality and disability rates[1,2]. sTBI results from a penetrating or blunt force injury to the brain that causes acute brain tissue damage. This is followed by a well characterized secondary injury cascade that persists for several months after the primary insult[3], culminating in significant tissue loss and cavitation. The secondary injury cascade includes edema, increased intracranial pressure, mitochondrial dysfunction, excitotoxicity, oxidative stress, and sustained pro-inflammatory signaling[4]. A major innate response observed in response to brain injury is the enhanced proliferation of neural stem cells (NSCs) in the NSC niche, which peaks at 24–48-hour post injury and results in their migration to the lesion site[5-7]. Despite their rapid response to injury, the regulatory mechanisms to prolong survival and promote neurotrophic NSC signaling are incapacitated by the pro-inflammatory microenvironment. Clinical management of sTBI focuses on stabilizing patients to reduce the spread of the secondary injuries associated with hypoxia and hypotension[8]. However, there are no clinically approved treatments to prevent the subsequent tissue and functional losses encountered after sTBI. In this dissertation, I explore the potential use of local and systemically administrable cell-free therapies that are designed to enhance endogenous repair responses and promote functional recovery after sTBI.

1.1 The NSC Microenvironment

NSCs are defined as mitotically active cells that have the ability to differentiate into neurons, astrocytes and oligodendrocytes[9]. Neurogenesis in the adult brain plays an important part in structural and functional plasticity[10]. The discovery of neurogenesis in the postnatal rodent brain in 1965[11] has led to a series of following studies that demonstrated the presence of NSCs in the adult brain[12-14]. Adult NSCs are tightly regulated within two distinct regions of the brain: the subventricular zone (SVZ) lining the ventricles and the subgranular zone (SGZ) of the dentate gyrus of the hippocampus. NSCs residing in the SVZ migrate via the rostral migratory stream to the olfactory bulb where they ultimately differentiate into granule interneurons, with minor contributions to the neocortex and basal ganglia[15,16]. NSCs in the adult SVZ differentiate into granule neurons, sending axons to CA3 pyramidal neurons[11,17].

Distinct structural and functional attributes of the NSC niche are responsible for protecting and regulating NSC maintenance[18]. Along with an intricate network of microvasculature[19], the highly specialized extracellular matrix (ECM) of the NSC niche that is rich in the lectican family of proteoglycans, plays a major role in sustaining NSC self-renewal and maintenance[20]. Lecticans consist of laterally emanating chains of sulfated chondroitin sulfate (CS) glycosaminoglycans (GAGs) that are covalently bonded to the core protein[20]. CS-GAG side chains are composed of repeating glucuronic acid (GlcA) and acetylgalactosamine (GalNAc) disaccharide units that can be sulfated at various positions as represented in figure 1.1 and further classified based on the precise sulfation patterns: O unit (GlcA-GalNAc), A unit (GlcA-GalNAc(4S)), C unit (GlcA-GalNAc(6S)), D unit (GlcA(2S)-GalNAc(6S)), and E unit (GlcA-GalNAc(4S, 6S))[21]. CS-GAG sulfation mediates both non-specific electrostatic interactions and "sulfation code"[22] specific interactions with soluble neurotrophic factors, fibroblast growth

factor, midkine and pleiotrophin, as well as their cognate receptors. Sulfated CS-GAGs also interact with neuronal guidance proteins, adhesion molecules, as well as cell surface receptors, serving multiple functions within the NSC niche[23]. The concentration and sulfation dependent binding of disulfated CS-E to various heparin-binding growth factors[24], and the orientation of sulfate groups in determining selectivity of binding[22], provide mounting evidence to suggest that the CS sulfation code is a key regulator of growth factor interactions and signaling in the NSC niche.

1.2 Endogenous Neurogenesis after sTBI

In response to injury, NSCs residing in the neurogenic niches significantly increase proliferation and migrate to the site of the injury[25,26]. However, the neuronal differentiation of endogenous NSCs is largely unsuccessful due to the prevailing pro-inflammatory microenvironment, which adversely affects NSC survival and differentiation. The primary injury to brain tissue results in axonal damage and hemorrhagic bleeding and disruption of the blood-brain barrier (BBB)[27]. Secondary injury to brain tissue is a consequence of the prolonged damage caused by excitotoxicity, mitochondrial dysfunction, oxidative stress, lipid peroxidation, neuroinflammation, axon degeneration and apoptosis[27]. The breakdown of the BBB and primary neuronal cell death are major contributing factors for excitotoxicity, which correlates with worsened functional outcomes[28]. Elevated levels of Ca^{2+} and reactive oxygen species leads to mitochondrial dysfunction, lipid peroxidation, and axonal degeneration, which further aggravates cell death[27]. Injured neuronal cells release damage-associated molecular patterns (DAMPs) and activate local microglia to trigger phagocytosis, followed by peripheral immune cells, such as neutrophils, monocytes, and T-cells[29]. Acute inflammatory response is required for debris clearance, neurotrophin production and barrier maintenance, but prolonged activation of

astrogliosis creates an unfavorable microenvironment for endogenous repair triggered by NSCs and the remaining cells[30]. The newly constructed ECM, commonly considered as astroglial scarring, is mainly composed of a mixture of resident activated glial cells, invading inflammatory cells, fibrous proteins, and GAGs[31]. Change in the ECM composition leads to tissue softening[32], and altered ECM architecture triggers neuropathological mechanotranduction, which affect cells within the perilesional area[33]. The secondary injury cascade is a complex series of molecular events that leads to significant brain tissue loss.

1.3 Current Progress in NSC-Based Therapies for sTBI

Clinical guidelines for the management of sTBI are focused on patient stabilization and prevention of the secondary injury cascades[34]. Treatment recommendations include decompressive craniectomy, prophylactic hypothermia, hyperosmolar therapy, cerebrospinal fluid drainage, ventilation therapies, sedatives, and seizure prophylaxis[34]. Rehabilitation interventions are recommended as soon as the condition of the patient allows[35]. Unfortunately, there are no approved treatments that can help alleviate the adverse effects of toxic microenvironment to promote tissue repair and regeneration after sTBI.

Preclinical studies have demonstrated the utility of NSCs as a cell-replacement therapy in multiple disease models, including TBI [36]. Direct transplantation of NSCs is an appealing therapeutic option for severe CNS injuries, and pre-clinical animal studies in both rodents and primates have demonstrated the feasibility of these procedures and their beneficial effects on mediating functional repair of the CNS [37-39 40,41]. Despite these advancements, NSC therapy for the injured CNS has so far not been translated to clinical practice. Increasing evidence indicates that transplanted NSCs show poor survival, and that the improved functional outcomes observed

after NSC transplantation may be the result of enhanced neurotrophic factors released by undifferentiated NSCs[42-44]. This bystander signaling mediated by undifferentiated NSCs is believed to locally enhance the availability of neurotrophic factors, such as nerve growth factor (NGF), brain derived neurotrophic factor (BDNF) and glial-derived neurotrophic factors (GDNF), that reduce scar formation and increase the survival of endogenous cells at the lesion site[36]. Furthermore, transplanted NSCs reduce inflammatory responses by secreting anti-inflammatory factors[36]. Hence, the conception of "cell-free" therapeutic approaches that can prolong the survival and integration of migratory endogenous NSCs, and potentiate the effects of NSC bystander signaling, can help prevent sTBI associated progressive tissue loss and restore function.

1.4 Strategies to Enhance Endogenous Neuroprotection and Regeneration following sTBI

Extracellular vesicles (EVs) are byproducts of the endocytic pathway, and carry cytosolic proteins, mRNAs, and miRNAs that are released into the extracellular space. EVs can be taken up by neighboring cells where they can activate paracrine signaling[45]. They are cost-effective to manufacture and do not carry the risk of teratoma formation, and can be injected intravenously (IV) without invasive surgeries. NSC-EVs have shown therapeutic potential by modulating inflammation and attenuating apoptosis in CNS injuries[46,47]. In Chapter 2, I tested the therapeutic efficacy of acute IV injections of NSC-EVs in male and female sTBI rats and demonstrated the sex-dependent neuroprotective effects of EV treatment at the tissue and functional levels.

Biomaterial scaffolds to provide cellular support and microenvironmental cues are also actively being pursued as a means of directly remodeling the injury microenvironment[48]. The overriding objective here is to protect NSC function and to drive differentiation of NSCs to

desired lineages for long-term functional integration. Our lab has previously demonstrated the advantages of utilizing CS-GAG-based hydrogels to recapitulate the neurogenic niche ECM, *in vitro*[49] as well *in vivo*[50,51]. Sulfated CS-GAG hydrogels possess the native functionality of CS in the neural ECM. They can bind trophic factors to promote the survival and proliferation of NSCs, reduce the damage to the tissue as well as the vasculature, and lead to enhanced functional recovery post-TBI. However, a detailed understanding of alterations in sulfation composition on NSC function is still lacking. I investigated the effect of CS-GAG sulfation on the regulation of NSCs *in vitro* (Chapter 3). I demonstrated the potential to either direct NSC maintenance or promote neuronal differentiation by modulating the extent of sulfation in CS-GAG hydrogels *in vitro*.

Clinical approaches to addressing sTBI deficits have been conservative in solely focusing on rehabilitative recovery measures[1]. This work studies explores new avenues of using cell-free approaches such as NSC-EVs and brain-mimetic sulfated CS-GAG hydrogels to modulate the injury microenvironment after sTBI. These approaches could be used synergistically to simultaneously influence various components of the endogenous repair cascade and provides patient-specific treatment options for sTBI in the future. In Chapter 4 of this dissertation, I summarize the results and implications of the findings.

1.5 References

1 Maas, A. I., Stocchetti, N. & Bullock, R. Moderate and severe traumatic brain injury in adults. *Lancet Neurol* **7**, 728-741, doi:10.1016/S1474-4422(08)70164-9 (2008).

2 Hukkelhoven, C. W. *et al.* Patient age and outcome following severe traumatic brain injury: an analysis of 5600 patients. *J Neurosurg* **99**, 666-673, doi:10.3171/jns.2003.99.4.0666 (2003).

3 Xiong, Y., Mahmood, A. & Chopp, M. Emerging treatments for traumatic brain injury. *Expert Opin Emerg Drugs* **14**, 67-84, doi:10.1517/14728210902769601 (2009).

4 Kaur, P. & Sharma, S. Recent Advances in Pathophysiology of Traumatic Brain Injury. *Curr Neuropharmacol* **16**, 1224-1238, doi:10.2174/1570159X15666170613083606 (2018).

5 Wang, X., Gao, X., Michalski, S., Zhao, S. & Chen, J. Traumatic Brain Injury Severity Affects Neurogenesis in Adult Mouse Hippocampus. *J Neurotrauma* **33**, 721-733, doi:10.1089/neu.2015.4097 (2016).

6 Ibrahim, S. *et al.* Traumatic Brain Injury Causes Aberrant Migration of Adult-Born Neurons in the Hippocampus. *Sci Rep* **6**, 21793, doi:10.1038/srep21793 (2016).

7 Imitola, J. *et al.* Directed migration of neural stem cells to sites of CNS injury by the stromal cell-derived factor 1alpha/CXC chemokine receptor 4 pathway. *Proc Natl Acad Sci U S A* **101**, 18117-18122, doi:10.1073/pnas.0408258102 (2004).

8 Dash, H. H. & Chavali, S. Management of traumatic brain injury patients. *Korean J Anesthesiol* **71**, 12-21, doi:10.4097/kjae.2018.71.1.12 (2018).

9 Song, H. J., Stevens, C. F. & Gage, F. H. Neural stem cells from adult hippocampus develop essential properties of functional CNS neurons. *Nat Neurosci* **5**, 438-445, doi:10.1038/nn844 (2002).

10 Toda, T. & Gage, F. H. Review: adult neurogenesis contributes to hippocampal plasticity. *Cell Tissue Res* **373**, 693-709, doi:10.1007/s00441-017-2735-4 (2018).

11 Altman, J. & Das, G. D. Autoradiographic and histological evidence of postnatal hippocampal neurogenesis in rats. *J Comp Neurol* **124**, 319-335 (1965).

12 Paton, J. A. & Nottebohm, F. N. Neurons generated in the adult brain are recruited into functional circuits. *Science* **225**, 1046-1048 (1984).

13 Richards, L. J., Kilpatrick, T. J. & Bartlett, P. F. De novo generation of neuronal cells from the adult mouse brain. *Proc Natl Acad Sci U S A* **89**, 8591-8595 (1992).

14 Eriksson, P. S. *et al.* Neurogenesis in the adult human hippocampus. *Nat Med* **4**, 1313-1317, doi:10.1038/3305 (1998).

15 Kornack, D. R. & Rakic, P. The generation, migration, and differentiation of olfactory neurons in the adult primate brain. *Proc Natl Acad Sci U S A* **98**, 4752-4757, doi:10.1073/pnas.081074998 (2001).

16 Altman, J. Autoradiographic and histological studies of postnatal neurogenesis. IV. Cell proliferation and migration in the anterior forebrain, with special reference to persisting neurogenesis in the olfactory bulb. *J Comp Neurol* **137**, 433-457, doi:10.1002/cne.901370404 (1969).

17 Altman, J. & Bayer, S. A. Migration and distribution of two populations of hippocampal granule cell precursors during the perinatal and postnatal periods. *J Comp Neurol* **301**, 365-381, doi:10.1002/cne.903010304 (1990).

18 Scadden, D. T. The stem-cell niche as an entity of action. *Nature* **441**, 1075-1079, doi:10.1038/nature04957 (2006).

19 Otsuki, L. & Brand, A. H. The vasculature as a neural stem cell niche. *Neurobiol Dis* **107**, 4-14, doi:10.1016/j.nbd.2017.01.010 (2017).

20 Ruoslahti, E. Brain extracellular matrix. *Glycobiology* **6**, 489-492, doi:10.1093/glycob/6.5.489 (1996).

21 Mikami, T. & Kitagawa, H. Biosynthesis and function of chondroitin sulfate. *Biochim Biophys Acta* **1830**, 4719-4733, doi:10.1016/j.bbagen.2013.06.006 (2013).

22 Gama, C. I. *et al.* Sulfation patterns of glycosaminoglycans encode molecular recognition and activity. *Nat Chem Biol* **2**, 467-473, doi:10.1038/nchembio810 (2006).

23 Djerbal, L., Lortat-Jacob, H. & Kwok, J. Chondroitin sulfates and their binding molecules in the central nervous system. *Glycoconj J* **34**, 363-376, doi:10.1007/s10719-017-9761-z (2017).

24 Deepa, S. S., Umehara, Y., Higashiyama, S., Itoh, N. & Sugahara, K. Specific molecular interactions of oversulfated chondroitin sulfate E with various heparin-binding growth factors. Implications as a physiological binding partner in the brain and other tissues. *J Biol Chem* **277**, 43707-43716, doi:10.1074/jbc.M207105200 (2002).

25 Rennert, R. C., Sorkin, M., Garg, R. K. & Gurtner, G. C. Stem cell recruitment after injury: lessons for regenerative medicine. *Regen Med* **7**, 833-850, doi:10.2217/rme.12.82 (2012).

26 Zheng, W. *et al.* Neurogenesis in adult human brain after traumatic brain injury. *J Neurotrauma* **30**, 1872-1880, doi:10.1089/neu.2010.1579 (2013).

27 Ng, S. Y. & Lee, A. Y. W. Traumatic Brain Injuries: Pathophysiology and Potential Therapeutic Targets. *Front Cell Neurosci* **13**, 528, doi:10.3389/fncel.2019.00528 (2019).

28 Chamoun, R., Suki, D., Gopinath, S. P., Goodman, J. C. & Robertson, C. Role of extracellular glutamate measured by cerebral microdialysis in severe traumatic brain injury. *J Neurosurg* **113**, 564-570, doi:10.3171/2009.12.JNS09689 (2010).

29 Shi, K., Zhang, J., Dong, J. F. & Shi, F. D. Dissemination of brain inflammation in traumatic brain injury. *Cell Mol Immunol* **16**, 523-530, doi:10.1038/s41423-019-0213-5 (2019).

30 Zhou, Y. *et al.* Dual roles of astrocytes in plasticity and reconstruction after traumatic brain injury. *Cell Commun Signal* **18**, 62, doi:10.1186/s12964-020-00549-2 (2020).

31 Kjell, J. & Gotz, M. Filling the Gaps - A Call for Comprehensive Analysis of Extracellular Matrix of the Glial Scar in Region- and Injury-Specific Contexts. *Front Cell Neurosci* **14**, 32, doi:10.3389/fncel.2020.00032 (2020).

32 Moeendarbary, E. *et al.* The soft mechanical signature of glial scars in the central nervous system. *Nat Commun* **8**, 14787, doi:10.1038/ncomms14787 (2017).

33 Hemphill, M. A., Dauth, S., Yu, C. J., Dabiri, B. E. & Parker, K. K. Traumatic brain injury and the neuronal microenvironment: a potential role for neuropathological mechanotransduction. *Neuron* **85**, 1177-1192, doi:10.1016/j.neuron.2015.02.041 (2015).

34 Carney, N. *et al.* Guidelines for the Management of Severe Traumatic Brain Injury, Fourth Edition. *Neurosurgery* **80**, 6-15, doi:10.1227/NEU.0000000000001432 (2017).

35 Brasure, M. *et al.* Participation after multidisciplinary rehabilitation for moderate to severe traumatic brain injury in adults: a systematic review. *Arch Phys Med Rehabil* **94**, 1398-1420, doi:10.1016/j.apmr.2012.12.019 (2013).

36 Martino, G. & Pluchino, S. The therapeutic potential of neural stem cells. *Nat Rev Neurosci* **7**, 395-406, doi:10.1038/nrn1908 (2006).

37 Ma, J. *et al.* Neural stem cell transplantation promotes behavioral recovery in a photothrombosis stroke model. *Int J Clin Exp Pathol* **8**, 7838-7848 (2015).

38 Tang, Y. *et al.* Neural stem cell protects aged rat brain from ischemia-reperfusion injury through neurogenesis and angiogenesis. *J Cereb Blood Flow Metab* **34**, 1138-1147, doi:10.1038/jcbfm.2014.61 (2014).

39 Wilcox, J. T., Satkunendrarajah, K., Zuccato, J. A., Nassiri, F. & Fehlings, M. G. Neural precursor cell transplantation enhances functional recovery and reduces astrogliosis in bilateral compressive/contusive cervical spinal cord injury. *Stem Cells Transl Med* **3**, 1148-1159, doi:10.5966/sctm.2014-0029 (2014).

40 Iwanami, A. *et al.* Transplantation of human neural stem cells for spinal cord injury in primates. *J Neurosci Res* **80**, 182-190, doi:10.1002/jnr.20436 (2005).

41 Redmond, D. E., Jr. *et al.* Behavioral improvement in a primate Parkinson's model is associated with multiple homeostatic effects of human neural stem cells. *Proc Natl Acad Sci U S A* **104**, 12175-12180, doi:10.1073/pnas.0704091104 (2007).

42 Einstein, O., Friedman-Levi, Y., Grigoriadis, N. & Ben-Hur, T. Transplanted neural precursors enhance host brain-derived myelin regeneration. *J Neurosci* **29**, 15694-15702, doi:10.1523/JNEUROSCI.3364-09.2009 (2009).

43 Pluchino, S. *et al.* Injection of adult neurospheres induces recovery in a chronic model of multiple sclerosis. *Nature* **422**, 688-694, doi:10.1038/nature01552 (2003).

44 Blurton-Jones, M. *et al.* Neural stem cells improve cognition via BDNF in a transgenic model of Alzheimer disease. *Proc Natl Acad Sci U S A* **106**, 13594-13599, doi:10.1073/pnas.0901402106 (2009).

45 Vogel, A., Upadhya, R. & Shetty, A. K. Neural stem cell derived extracellular vesicles: Attributes and prospects for treating neurodegenerative disorders. *EBioMedicine* **38**, 273-282, doi:10.1016/j.ebiom.2018.11.026 (2018).

46 Zhang, G. *et al.* Exosomes derived from human neural stem cells stimulated by interferon gamma improve therapeutic ability in ischemic stroke model. *J Adv Res* **24**, 435-445, doi:10.1016/j.jare.2020.05.017 (2020).

47 Rong, Y. *et al.* Neural stem cell-derived small extracellular vesicles attenuate apoptosis and neuroinflammation after traumatic spinal cord injury by activating autophagy. *Cell Death Dis* **10**, 340, doi:10.1038/s41419-019-1571-8 (2019).

48 Wang, Y., Tan, H. & Hui, X. Biomaterial Scaffolds in Regenerative Therapy of the Central Nervous System. *Biomed Res Int* **2018**, 7848901, doi:10.1155/2018/7848901 (2018).

49 Karumbaiah, L. *et al.* Chondroitin Sulfate Glycosaminoglycan Hydrogels Create Endogenous Niches for Neural Stem Cells. *Bioconjug Chem* **26**, 2336-2349, doi:10.1021/acs.bioconjchem.5b00397 (2015).

50 Betancur, M. I. *et al.* Chondroitin Sulfate Glycosaminoglycan Matrices Promote Neural Stem Cell Maintenance and Neuroprotection Post-Traumatic Brain Injury. *ACS Biomater Sci Eng* **3**, 420-430, doi:10.1021/acsbiomaterials.6b00805 (2017).

51 Latchoumane, C. V. *et al.* Engineered glycomaterial implants orchestrate large-scale functional repair of brain tissue chronically after severe traumatic brain injury. *Sci Adv* **7**, doi:10.1126/sciadv.abe0207 (2021).

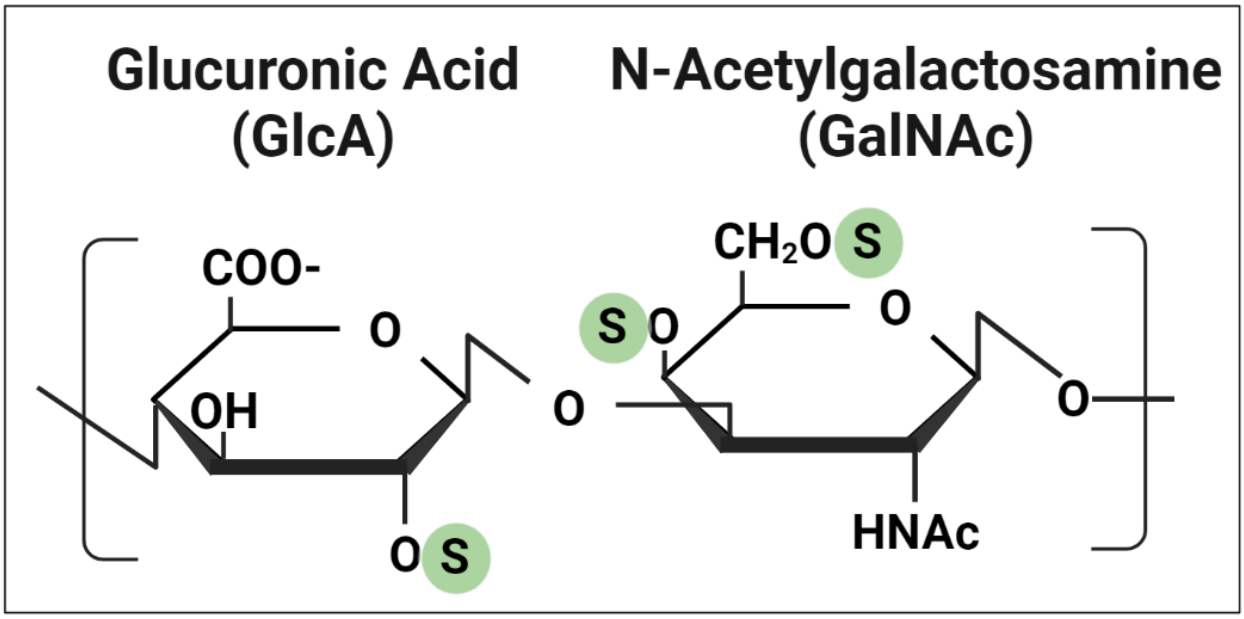

Figure 1.1 CS chains are composed of repeating glucuronic acid (GlcA) and N-acetylgalactosamine (GalNAc) disaccharide units that can be esterified by sulfate at various positions as indicated by “S” enclosed by a circle.

CHAPTER 2

EXTRACELLULAR VESICLES MEDIATE NEUROPROTECTION AND FUNCTIONAL RECOVERY AFTER TRAUMATIC BRAIN INJURY[1]

[1] Sun, M. K., Passaro, A. P., Latchoumane, C., Spellicy, S. E., Bowler, M., Goeden, M., . . . Karumbaiah, L. (2020). *Journal of Neurotrauma, 37*(11), 1358-1369. Reprinted here with permission of publisher.

Abstract

The lack of effective therapies for moderate-to-severe traumatic brain injures (TBIs) leaves patients with lifelong disabilities. Neural stem cells (NSCs) have demonstrated great promise for neural repair and regeneration. However, direct evidence to support their use as a cell-replacement therapy for neural injuries is currently lacking. We hypothesized that NSC–derived extracellular vesicles (NSC EVs) mediate repair indirectly after TBI by enhancing neuroprotection and therapeutic efficacy of endogenous NSCs. We evaluated the short-term effects of acute intravenous injections of NSC EVs immediately following a rat TBI. Male NSC EV-treated rats demonstrated significantly reduced lesion sizes, enhanced presence of endogenous NSCs, and attenuated motor function impairments four weeks post-TBI, when compared to vehicle- and TBI-only male controls. Although statistically not significant, we observed a therapeutic effect of NSC EVs on brain lesion volume, nestin expression and behavioral recovery in female subjects. Our study demonstrates the neuroprotective and functional benefits of NSC EVs for treating TBI and points to gender-dependent effects on treatment outcomes, which requires further investigation.

Key words (<5): TBI, neural stem cell, extracellular vesicles, neuroprotection

2.1 Introduction

Moderate-to-severe traumatic brain injuries (TBIs) have an estimated financial burden of over $70 billion per year due to the permanent disability and medical costs associated with the injury[1], making it a major public health problem. TBI severity depends not only on the extent of primary brain tissue damage, but also on the secondary molecular injury cascades, which can persist for several months to years following a TBI, exacerbating tissue damage and dysfunction, and contributing to the reduced life expectancy of TBI survivors[2]. Therapeutic interventions during the acute phase of TBI are therefore crucial to minimizing secondary injury and improving prognosis [3].

Neural stem cell (NSC) transplantation has been actively explored as a means to replace lost neurons and reduce secondary injury after TBI[4]. Although acute functional benefits were demonstrated in these studies[5,6]; immune rejection, low cell engraftment, as well as the invasive delivery of transplanted NSCs remain major challenges that need to be overcome in order to achieve chronic functional recovery[4]. In parallel to these issues, a growing body of recent evidence also suggests that NSCs are more likely promoting functional recovery not directly via cell-replacement and differentiation, but indirectly via "bystander" signaling mediated by NSC-secreted factors and paracrine mechanisms[7]. Previously, NSC EV treatment has demonstrated its therapeutic benefit in promoting neural tissue preservation and functional recovery after ischemic stroke in mouse and pig models[8,9]. Intravenously (IV) administered NSC EVs preferentially accumulate at the injury penumbra, directly come in contact with injured cells, and are suspected to be taken up by recipient cells[8]. NSC EVs do not pose threats associated with uncontrolled growth or immune rejection and are able to cross the blood-brain barrier (BBB) [10], which allows for less invasive methods of delivery and repeated treatments if desired. Due to their

neuroprotective and immunomodulatory properties, NSC EVs could present a viable "cell-free" therapy for TBI and an alternative to direct stem cell transplantation.

Sexual dimorphism between male and female brains contributes to sex-dependent differences in outcomes following TBI, indicating a difference in brain repair and compensatory mechanisms[11]. A number of clinical studies report worsened TBI outcomes in women than in men, with increased risk of death in women experiencing moderate-to-severe TBIs[12,13]. Sexual dimorphism in TBI pathology is also reflected in the altered microglial and macrophage activation patterns in males versus females as reported in recent preclinical studies[14,15]. However, in contrast to the above reports, the neuroprotective effects of female hormones such as estrogen and progesterone have also been linked to reduced mortality after TBI in women when compared to age-matched men[16]. The complex pathophysiological manifestations of different TBI types along with the sex-dependent changes in brain structure, chemistry, neuroinflammation, and recovery, warrant the need for better preclinical study-design criteria in order to comprehensively understand the sex-dependent manifestations of TBI and the effects of novel therapeutics on recovery.

In this study, we conducted controlled cortical impact (CCI) injuries to the rat motor cortex and intravenously administered size-constrained NSC EVs to male and female rats acutely post-TBI. We longitudinally assessed functional recovery using a beam-walk test over a four-week period and performed terminal immunohistochemical assessments to quantify changes in lesion size, scar formation, NSC presence, and angiogenesis.

2.2 Materials and Methods

Extracellular vesicle isolation. Human embryonic H9 cells were differentiated into NSCs using standard procedures previously published[9]. Medium was harvested from NSC cultures every 24

hours from a single passage. Media was filtered through a 0.22 µm filter and then further enriched by ultrafiltration using a Tangential Flow Filtration (TFF) system (all from Spectrum Laboratories, Rancho Dominguez, CA) and filtrate was subsequently washed with 10 X HyClone^{TM} DPBS (Thermo Fisher Scientific). NSC EV size and concentration were verified using nanoparticle tracking analysis via a NanoSight NS300 instrument (Malvern Panalytical, Malvern, UK). NSC EVs were diluted 1:100 in PBS, mixed thoroughly via trituration, and advanced through the microfluidic detection chamber at a controlled rate using a syringe pump. Analysis was performed using NTA software (Malvern), and reported values are average values from 5 individual 60 second recordings (Supplementary Fig. 1). The resulting concentrated extracellular vesicles were aliquoted and stored at -20°C until needed for treatments.

In vitro scratch wound assay. A scratch wound assay was performed using procedures adapted from previously published methods[17]. Briefly, human neural progenitor cells (hNP1; ArunA Biomedical, Inc., Athens, GA) were cultured and expanded as described above and passaged onto 24-well plates (Fisher Scientific, Waltham, MA) coated with Matrigel (Corning, Corning, NY). When confluent, a vertical scratch was made through the center of each well using a P200 pipette tip (Mettler Toledo, Columbus, OH). Culture media was replaced with fresh media either with or without the addition of NSC EVs (approximately 2 x 10^8 EVs/well), and wells were imaged immediately and at the same locations 48 hours later. The area of the "scratch wound" was calculated using ImageJ (NIH, Bethesda, MD) by outlining the area without cells and using the "Measure" function on all images, and closure was calculated by dividing the area at T0 by the area at T48. Experiment was repeated thrice (n=10).

Controlled cortical impact (CCI) induced TBI of the rat motor cortex. All animal work and procedures were approved by the University of Georgia Institutional Animal Care and Use

Committee (IACUC) and were in accordance with the National Institutes of Health (NIH). Power analysis on preliminary animal behavior and tissue changes indicated that n = 7 per group would be sufficient to reach a cut off of 1 - ß = 0.8. We then included n = 8 rats per group to account for optimal reduction of effect size and for additional variability in our assays. 24 male, and 24 female adult Sprague-Dawley rats (250~270g; Envigo) were randomly assigned to one of the following groups: (1) CCI [18] control (male =8, female=8), [19] vehicle (isotonic PBS)-treated (male =8, female=8), and (3) NSC EV-treated group (male =8, female=8). A focal CCI injury was induced using a custom-built pneumatic impactor that has been characterized by us previously[20]. Briefly, the animal was anesthetized with 2-3% isoflurane, and received a craniotomy to expose the left hind limb motor cortex region in the right hemisphere (bregma 0, 1.5mm lateral from the midline as the center of the impact)[21]. A 3mm diameter tip was pneumatically actuated at an average velocity of 2.17m/s with the average cortical dwell time of 250 msec to create an injury depth of 2mm. Excess blood was removed, and the craniotomy site was covered with 0.5% sterile seakem agarose (Lonza, NH). The incision was closed using nylon fiber sutures (ACE, MA). NSC EV-treated and vehicle-treated rats received three doses of either NSC EV (4e10EVs/kg in 1.6 mL) or vehicle (isotonic PBS; 1.6 mL) via tail vein using a 3mL syringe attached to a 26G needle at 4-6 hour, 24-26 hour, and 48-50 hour post-CCI. The volume injected was necessary (given our TFF system EV concentration efficiency) to achieve the desired dose of 4e10 EVs/kg, which was chosen based on our previous *in vivo* EV studies[8,9].

Motor Function Assessments. The animal's fine motor coordination and ability to maintain balance were assessed via a beam walk test. All animals were trained for 3 consecutive days prior to CCI, and the performance was measured on 4, 7, 14, 21, and 28 days post-CCI. The animal was placed at the bottom of a 1-meter-long beam tilted at 30 degrees angle and allowed to climb up the beam

into a black box located at the end of the beam. The number of foot faults, falls, as well as the time to complete the task and final distance climbed were documented. Data was analyzed by the primary experimenter and confirmed by a second experimenter via video recording. All experimenters and animal handlers were blinded to treatment groups. One outlier in each male group (NSC EV-treated, vehicle and control) were detected using univariate approach (Rstudio Inc., MA), confirmed using expected behavioral impact of TBI and excluded from analysis.

Tissue Collection. Four weeks post-CCI, animals were euthanized via transcardial perfusion with 4% paraformaldehyde. Once the perfusion was completed, the brain was extracted and incubated in PBS with 30% sucrose at 4 °C until saturated. It was embedded in Optimal Cutting Temperature compound (Thermo Fisher, NH) and flash frozen in liquid nitrogen. Extracted brains were sectioned at 15 μm thickness using a cryostat (LeicaBiosystems, IL).

Hematoxylin and eosin (H&E) staining. Hematoxylin and eosin staining (H&E) was used to determine the lesion area of the coronal sections between bregma +0.5mm and -0.5mm. The "Measure" function in ImageJ (NIH, Bethesda, MD) was used to calculate the area of the lesion by overlaying the contralateral hemisphere to the injured hemisphere, and outlining the missing tissue (N=96, 48 animals, 2 sections per animal). Remaining tissue was estimated as a lost tissue area in mm^2 and percentage of remaining intact cortex. An outlier in male NSC EV-treated animal was detected using the univariate approach (Rstudio Inc., MA) and excluded from analysis.

Immunohistochemistry. Non-consecutive sections were rinsed with PBS three times and incubated in blocking buffer (PBS with 0.5% Triton-X100 containing 4% bovine serum albumins or 4% goat serum) for an hour. Sections were then incubated in blocking buffer containing primary antibodies against GFAP (Z0334; 1:500), NeuN (ABN91; 1:500), CD68 (MCA341R; 1:100), RECA-1 (MCA970R; 1:200), COL IV, nestin (AF2736; 1:1000), Sox1 (ab87775; 1:500) and Flk-1 (sc-315;

1:250) overnight at 4°C. The next day, sections were rinsed with washing buffer (PBS with 0.5% Triton-X100) three times followed by an hour of blocking. Sections were incubated in blocking buffer containing AlexaFluor 488 (Life Technologies, CA), AlexaFluor 555 (Life Technologies, CA), and AlexaFluor 647 (Life Technologies, CA) for secondary binding. The sections were rinsed again with washing buffer, counterstained with NucBlue (Life Technologies, CA), and mounted with fluoromount-G (SouthernBiotech, AL). Images were obtained using the Leica DM microscopy system (Leica Microsystems Inc., IL). Volocity software (PerkinElmer, MA) was used to process the raw images obtained for fluorescence expression. GFAP line intensity values were obtained using the MATLAB Image Processing Toolbox (Mathworks, MA)[22]. n=5 (2 slides/animal, total 30 animals x 2 slides = 60 slides) was used for GFAP intensity analysis.

Composite Scores. For all groups, a total of 11 variables were obtained from behavioral assessments at day 28 (Beam walk completion time, distance, number of falls, left hindlimb faults, right hindlimb faults, left forelimb faults and right forelimb faults) and histological data (Lesion volume, nestin, VEGFR2, and GFAP expression). We then computed composite scores summarizing the overall recovery of the animals using two popular dimensionality reduction methods (R-package): The Fisher linear discriminant analysis [23] and principal component analysis (PCA). Using a linear classifier (Multivariate normal density fitting with a pooled estimate of covariance; Mathworks, Inc.) and a leave-one-out cross-validation approach, we computed the accuracy (true positive over total sample in percentage) and the sensitivity (true positive over the sum of true positive and false negative, in percentage) to assess the best separating variable combination. The dimensionality reduction approaches used the first two components with the highest explained variance for both LDA and PCA. Classification results were computed separately for male and female data.

Statistical Analysis. For all group comparison, Kolmogorov-Smirnov and Levene's tests were performed to test for normality and equality of variance, respectively. When sample size and normality were verified, parametric tests were performed for two or three sample comparisons (Student t-test, one-way ANOVA), and non-parametric tests were used otherwise (i.e. Wilcoxon rank sum test, ANOVA on ranks). For multiple factor conditions, two-way ANOVA and repeated measure ANOVA (rmANOVA) were performed. Post-hoc multiple comparisons were performed using Holm-Sidak test, which adjusts the significance level for multiple comparisons and provides tighter bounds. Holm-Sidak test can be used for both pairwise comparisons and comparisons versus a control group. Tukey nonparametric comparison was used as a post-hoc test in ANOVA on ranks. Pearson's correlation was used for correlations between VEGFR2 percentage expression area and nestin percentage expression area. A p-value lower than 0.05 was considered significant and all statistical tests were performed using Sigmaplot (Systat Software, Inc., CA) and R-studio (RStudio Inc.,MA). All values are reported as mean ± SEM and n=8 per group unless otherwise specified.

2.3 Results

NSC EV treatment reduced lesion volume in both males and females.

We examined whether acute intravenous administration of NSC EVs would help to reduce TBI lesion area in a rat TBI model. Rats received a CCI injury targeting the left hind limb motor cortex, followed by three NSC EV injections at 6h, 24h, and 48h intervals of either NSC EVs or vehicle (isotonic PBS; Fig. 1). Isotonic PBS was chosen as the vehicle in accordance with standard EV isolation protocols (see Methods), and TBI control rats did not receive any injections. We terminally quantified the average lesion area for each group at the end of four weeks (Fig. 2). Using

direct quantification of the lost tissue area at 4 weeks post-injury compared to the contralateral hemisphere (Fig. 2D), we observed a decreased lesion area in NSC EV-treated males (1.675±0.398 mm^2; p=0.011, one-way ANOVA) compared to vehicle-treated males (2.147±0.308 mm^2; p = 0.054) and control TBI males (3.237±0.193 mm^2; p = 0.011). We detected a marginal increase in spared tissue (spared tissue as a percentage of remaining cortex; Fig. 2F, G, and H) in the NSC EV-treated group (Fig. 2I; 90.692±2.192%) compared to both vehicle-treated (89.052±1.986%) and TBI control (89.925±1.400%) males. NSC EV-treated females also demonstrated reduction in lesion sizes and increase in spared tissue, although no significant differences were found (Fig. 2E and Fig. 2J; p=0.250, one-way ANOVA). Additionally, in contrast to TBI control and vehicle-treated rats, which mostly exhibited tissue cavitation at the site of impact (Fig. 2B and C), NSC EV-treated rats exhibited maintenance of the cortical structure with a majority of the tissue consisting of CD68+ and GFAP+ cells and a minority of NeuN+ cells (Fig. 2A).

NSC EV treatment had little effect on Glial Fibrillary Acidic Protein (GFAP) expression.

We quantified the fluorescence intensity of GFAP+ astroglial scar across all groups and treatments using lines drawn perpendicularly to the tangent of the TBI penumbra (Fig. 3A) and plotted the integrated GFAP+ intensity as the intensity summation over a distance of 160 μm (Fig. 3B, E). Expectedly, we observed a monotonic decrease in GFAP expression from the site of injury over a 160 μm distance across all treatment groups (Fig. 3B, E). Average GFAP expression in the perilesional area showed no significant difference in males (p=0.281, ANOVA on ranks, Fig. 3C). However, male vehicle-treated rats (0.0574±0.0172) expressed relatively higher expression of GFAP indicating thicker scarring of the tissue, in comparison to NSC EV-treated (0.0386±0.0135) and control (0.0324±0.0082). No treatment effect was also detected on GFAP expression among female groups (p=0.181, ANOVA on ranks, data not shown). Interestingly, the overall GFAP

intensity was higher in female TBI control (0.0739±0.0197) rats, when compared to male TBI control (0.0324±0.0082, p=0.0422, t-test; Fig. 3 D, E, F).

NSC EV treatment enhanced the presence of NSCs near the lesion site.

We quantified the effects of NSC EV treatment on the presence of NSCs around the site of injury using nestin immunostaining (Fig. 4). Expression of Nestin in NSC EV-treated male rats at the perilesional area was significantly enhanced (Fig. 4C; 4.01±0.66%; p=0.011, one-way ANOVA) when compared to the TBI control male rats (1.54±0.61%; p = 0.014, Bonferroni Test), while a strongly trending increase was also observed when compared to vehicle-treated male rats (2.00±0.31%; p=0.053, Bonferroni Test). Nestin expression among female groups exhibited a moderate trend in the same direction, with relatively higher nestin expression observed in NSC EV-treated female rats (Fig. 4D; 4.35±0.66%), followed by vehicle-treated (3.06±0.70%), and TBI control female rats (2.44±0.68%); however, these results were not quite statistically significant despite the moderate trend (p = 0.145, one-way ANOVA). These results suggest that NSC EV promoted endogenous NSC migration to the site of injury in males, a response to injury that has been noted previously[24]. In order to test this hypothesis, we performed 2D scratch wound assays on human NSCs and quantified NSC EV-dependent cell migration (Supplementary Fig. 2). We observed that NSC EV treatment significantly increased migration into the scratch-induced lesion at the end of 48 h, with an average closure of 60.0 ± 3.5% observed in the NSC EV-treated group when compared to 48.2 ± 3.7% (Supplementary Fig. 2E; p=0.0244, two-tailed t-test) for the untreated control group. These results indicate that NSC EV treatment enhanced the cell migration within the scratch induced lesion, which supports the hypothesis that the increase in nestin-positive cells observed in the perilesional area is due to enhanced migration of endogenous NSCs to the injury site.

NSC EV treatment enhanced VEGFR2 expression around the lesion site in male rats.

To analyze the effects of NSC EV treatment on angiogenesis and vascular density, we quantified the expression of sprouting endothelial cell marker, vascular endothelial growth factor receptor 2 (VEGFR2/Flk-1/KDR); as well as total endothelial markers, RECA-1 and collagen IV (Col-IV), via immunohistochemistry (Fig. 5). In males, the NSC EV-treated group exhibited significantly increased VEGFR2 expression (Fig. 5F; 4.84±0.40%; $p = 0.038$, one-way ANOVA) when compared to the TBI control (2.99±0.58%; $p = 0.047$, Bonferroni) group and moderately increased VEGFR2 expression compared to the vehicle-treated (3.39±0.50%; $p = 0.155$, Bonferroni) group. In contrast, we did not observe differences in RECA-1 or Col-IV expression ($p = 0.267$, and $p = 0.479$, respectively, one-way ANOVA, n=5 per group). In females, we did not detect any statistical differences in VEGFR2, RECA-1, or Col-IV ($p = 0.617$, $p = 0.941$, $p = 0.525$, respectively; one-way ANOVA; n=8, 5, 5, respectively) among the groups. Although NSC EV treatment significantly increased VEGFR2 expression in males, this increase did not result in a detectable increase of total vascular density at the four-week experimental end point as determined by RECA-1 and Col-IV expression. Interestingly, a positive correlation was revealed between VEGFR2 and nestin expression in male animals (Supplementary Fig. 3A; $r=0.632$, $p=0.001$, Pearson), while in females, no trend was detected (Supplementary Fig. 3B; $r=-0.049$, $p=0.820$, Pearson).

NSC EV treatment improved motor function recovery in male rats.

Motor recovery of rats was assessed over a four-week period using a beam-walk test to assess the impact of NSC EV injection on functional recovery in animals (Fig. 6). We observed a reduced number of left hind limb faults in NSC EV-treated male rats on day 4 post-TBI (Fig. 6A; 2.52±0.16; two-way RM ANOVA), when compared to the TBI control (6.19±1.51; $p=0.046$,

Holm-Sidak) group, but only a slight, non-significant reduction compared to the vehicle-treated group (4.19±1.88; p=0.258, Holm-Sidak). The difference in the number of left hind limb faults among groups decreased over time, following a similar recovery trajectory.

Both lesion area and left hind limb foot faults exhibited similar trends among groups, with the NSC EV-treated group retaining moderately more cortical tissue than the vehicle-treated and control groups as well as exhibiting slightly fewer left hind limb faults. As it stands to reason that these variables may be correlated, with a larger lesion correlating to an increased number of foot faults, we performed a regression analysis to examine these correlations among groups (Supplementary Fig. 4). The NSC EV-treated group showed a moderate correlation (r=-0.567, p=0.185) with a strong negative slope, reflecting the expected relationship. The other two groups, however, have milder slopes, suggesting that for a given lesion size, NSC EV-treated animals tend to show improved recovery (fewer left hind limb faults). While more investigation is needed to determine mechanisms, these results indicate that NSC EV treatment provides recovery benefits that cannot solely be predicted by lesion area or left hind limb faults.

In accordance with our histological data, female rats demonstrated a rather complex recovery trend that was quite different from that observed in males (Supplementary Fig. 5A). Statistically significant differences were not detected on any tested day due to large variability within female treatment groups. Together, these results indicate that NSC EV injection acutely improved motor function recovery in NSC EV-treated males.

Linear discriminant analysis [23] demonstrated clustering of male NSC EV-treated rats.

We used principal component analysis[25] (PCA) and linear discriminant analysis [23,26] in an effort to reduce biomarkers (total number of markers = 11; sample size = 24) and achieve integrated visualization of changes following treatments (Fig. 6B, C, D). We limited our analysis

to the first two components (Fig. 6B; correlation matrix-based model) of PCA and LDA modeling over the last day of the experiment (28 days) for correspondence between behavioral measures and histology. Classification using raw data (37.5% accuracy, 60.0% sensitivity), PCA-derived values (29.2% accuracy, 53.8% sensitivity) and LDA-derived values (75.0% accuracy, 53.8% sensitivity) suggested LDA dimensionality reduction captures the effect of NSC EV treatment the best and was able to separate the group difference based on the given variables (Fig. 6B). We observed that the linear discriminant 1 (LD1, 80.12% explained variable) showed a significant separation in treatment groups (Fig. 6C, D; $p < 0.001$, one-way ANOVA) in males but not females (Supplementary Fig. 5). The LD1 major contribution was observed to be from variables measured in VEGFR2 and nestin expression. This result indicates enhanced NSC mobilization is the major contributing factor in the recovery of NSC EV-treated males.

2.4 Discussion

NSC therapy has long been considered to hold great promise for TBI, although, much of this evidence has been restricted to pre-clinical animal studies. The lack of clinical translation of NSC and other cell-based therapies for TBI could be attributed to an inadequate understanding of the mechanisms of repair, which, unlike pharmacological monotherapies, are multifaceted. Evidence suggests that NSC-mediated repair and neuroprotection takes effect not only due to cell replacement, but largely via secreted growth factors and NSC EVs carrying therapeutic genes and proteins[27,28]. NSC EVs carry a cargo of neuroprotective proteins and RNA that have the potential to modulate the gene expression of recipient injured cells[29], which is one of the main therapeutic mechanisms of transplanted NSCs[30]. NSC EVs do not require the same degree of technical skill, time, and expense that is required for NSC expansion, storage, and handling[31], but confer similar

functional benefits and modulation of the injury environment[32]. For all these reasons, NSC EVs have enormous potential for clinical translation. In this study, we explored the acute neuroprotective and functional benefits of administering NSC-derived NSC EVs acutely after TBI and observed acute sex-dependent neuroprotective effects of intravenously-delivered NSC EVs in age-matched male and female rats.

The substantial brain tissue loss that occurs immediately and in the days-to-weeks following a TBI leads to significant long-term functional impairments. Protecting the brain from undergoing long-term damage has been the focus of several pre-clinical and clinical studies. However, pharmacological agents designed to promote neuroprotection have largely failed in clinical trials, likely due to inadequate consideration of TBI severity, timing of administration and route of delivery, temporal assessment of functional outcomes, and the effects of age, sex, and other dependent variables[33]. In the case of TBI, reduced time to definitive care leads to a better recovery trajectory[34]. Further, temporal delays due to inaccessibility to emergency care, or time lost during injury evaluation could have significant long-term implications[35,36]. The administration of NSC EVs could potentially serve as an effective neuroprotective agent in the critical care setting. Here, the neuroprotective effects of NSC EV treatment was demonstrated via significant behavioral and tissue level changes, including reduction of lesion size and increased VEGFR2 and nestin expression four weeks post-TBI. Interestingly, the analysis of lesion area in female rats revealed a large variation in therapeutic effect across groups, which may be related to the unsynchronized estrous cycle of female rats at the time of the CCI. Since female sex hormone concentrations at the time of injury induction has been demonstrated to have a prominent impact on TBI outcome[37,38], fluctuating hormone levels in female rats may have masked the treatment effects of NSC EVs.

Antibodies against the filamentous glial fibrillary acidic protein (GFAP) are commonly used to mark activated astrocytes, which coalesce to form astroglial scar around CNS injuries[39]. The dogma that astroglial scarring inhibits axonal regeneration is now in debate. Contrary to its neurite-inhibiting qualities, the potential benefit of astroglial scarring in axon regeneration was recently demonstrated in spinal cord lesions[40]. TBI induces clear gradients in the expression of reactive astrocytes from the injury site[41]. These astrocytes are highly heterogeneous and are proposed to perform complex functions in immune modulation, BBB regulation, and neural circuit reorganization[41]. Since hypertrophic reactive astrocytes selectively upregulate GFAP as a function of distance from the lesion site, we used line intensity analysis to accurately capture the spatial distribution of GFAP staining intensity from the lesion boundary to the perilesional space[42]. Our results demonstrated that NSC EVs neither enhance nor reduce the expression of GFAP at the lesion site and this expression has no major implication in NSC EV mediated-recovery. We speculate that this lack of difference in GFAP expression is likely due to the sub-acute, four week time course of study and due to the fact that scar composition and pro-inflammatory responses are still evolving during this period[43,44]. Disparity between GFAP expression in male and female control TBI rats is expected due to fundamental structural differences in male and female brains[45]. Studies addressing sexual dimorphism in glial activation following TBI suggest that inflammatory responses, including glial activation, differ in male and female brains. When compared to males, the age and estrous cycle of females are known to directly influence the increase, decrease, or maintenance of local GFAP expression at the lesion site[15,46]. This complex regulation of GFAP response in female subjects makes it challenging to interpret the role of GFAP expression in terms of injury recovery outcome. Our study implies that GFAP expression associates differentially to functional recovery in male rats versus female rats following TBI. Although GFAP is widely

accepted as a pro-inflammatory astroglial scarring response following TBI in pre-clinical studies, our results suggest that it is not a strong indicator of recovery at the 4 week sub-acute endpoint after TBI as evaluated in this study.

EVs derived from mesenchymal stem cells (MSCs) have been previously shown to increase cell migration of multiple cell types[47,48]. In addition, the presence of integrin involved in regulation of cell migration has recently been reported in NSC EVs[8,49]. This observation, taken together with considerable evidence demonstrating that endogenous TBI repair mechanisms involve NSC migration to the perilesional area[50], is suggestive of the role of NSC EVs in enhancing endogenous NSC migration to the site of the injury. We have previously demonstrated the proclivity of NSC EVs to home to injured brain tissue in a rodent stroke model[51]. Homing of NSC EVs to the lesion site suggests that NSC EVs may also contribute locally to neuroprotection and improved therapeutic outcomes, though further exploration is needed to determine specific mechanisms underlying these benefits. This implication also supports the suggestion that endogenous migrated NSCs exert neuroprotective effects at the lesion site via secretion of endogenous NSC EVs. Indeed, while endogenous migration was not directly examined, analysis of in vivo nestin immunohistochemistry (Fig. 4) in combination with the in vitro scratch wound assay (Supplementary Fig. 2) strongly suggested that NSC EVs promoted endogenous NSC migration. This increased presence of NSCs in the perilesional area could be one of the contributing factors to neuroprotective outcomes, as has been shown previously[24]. An increase in NSC migration to the injured area may contribute to recovery via enhanced neurogenesis and paracrine effects, including endogenous NSC EV secretion from the migrated cells, similar to the repair mechanisms that have been reported in previous TBI studies[52]. An increased level of proliferation and neurogenesis at the NSC niche and migration of NSCs to the injured cortex area have been reported

after TBI[50]. Stem cell-derived NSC EVs have been demonstrated to enhance endogenous neurogenesis and neurite outgrowth by miRNA transfer[53], suggesting miRNA transfer as a likely mechanism. However, the heterogeneity of NSC EV content renders the identification of a specific molecular pathway that leads to enhanced NSC migration challenging. Our results support these previous findings and suggest that NSC EV treatment directly contributes to the proliferation of locally-recruited NSCs, likely via similar mechanisms as reported previously. Further investigation is necessary to identify and characterize the relevant cargo in NSC EV for a better understanding of the mechanisms involved.

VEGF mediates many different receptor-specific functions, and binding of VEGF/VEGFR2 is implicated in elevation of mitogenic and angiogenic activities[54]. VEGFR2 expressed in endothelial cells increases proliferation and migration upon binding, leading to neovascularization and vasculature rearrangement. Similarly, VEGFR2 expressed in NSCs supports the proliferation and migration of NSCs[55]. Furthermore, upregulation of VEGF and VEGFR2 around the lesion is associated with post-traumatic angiogenesis and neurogenesis after TBI[56,57]. We observed a positive correlation between VEGFR2 and nestin expression around the site of injury in NSC EV-treated rats (Supplementary Fig. 3A) potentially suggesting an increase in VEGFR2-dependent NSC proliferation and recruitment after TBI, though NSC proliferation was not directly measured in this study. Although there was no detectable increase in vasculature density in the perilesional area, we cannot exclude the modulatory role VEGF plays on functional remodeling of vasculature, and vascular permeability[58]. Taken together, NSC EV treatment increased VEGF/VEGFR2 activity, which we speculate may contribute to neuroprotection.

Since TBI lesions were induced in the primary motor cortex, we investigated the behavioral performance on a motor task and correlated the tissue-level changes to functional recovery

following TBI. Overall, NSC EVs had an acute effect in reducing the severity of functional deficits over a four-week period compared to the control group in males (Fig. 6). Pre-clinical and clinical studies for cell-based therapies have investigated the underlying mechanisms of stem cell-initiated cognitive and motor function recovery and confirmed that cell replacement is not the sole means of injury repair[59]. The release of anti-inflammatory trophic factors, as well as gene and protein transfer by NSCs have also been reported to contribute to functional repair of TBI[28]. In addition to systemically-delivered NSC EVs, endogenous NSCs that migrate to the lesion site, which were identified via nestin expression, likely contribute to bystander signaling. Hence, functional recovery of TBI animals can be credited to direct the neuroprotective paracrine effect of NSC EVs, in combination with the endogenous NSC bystander effect indirectly enhanced by NSC EV treatment.

Using LDA, we assessed the combined effect of NSC EV treatment on immunohistochemical and behavioral changes. Females demonstrated no distinguishable differences in response to NSC EV treatment, while male NSC EV-treated rats showed separation from both the vehicle-treated and TBI control groups. In combination with individual null hypothesis testing (NHT)-based assessment, we confirmed that NSC EV treatment has a marked beneficial effect on male rats. The contributing variables that carried most of the weight in LD1 were related to the beam-walk test, indicating that NSC EV treatment had a pronounced effect on motor recovery that isolated NSC EV-treated rats from the other groups. Although individual beam-walk measurements may not appear significant in NHT-based tests, combining these measurements allowed us to reduce the intrinsic noise collected from biological data, and helped evaluate the true treatment effects.

In this study, the vehicle-treated male rats (injection control group) demonstrated an unexpected positive behavioral recovery, with trends that aligned closer to NSC EV-treated rats rather than TBI control rats at later time points (day 14, 21, 28), which is also reflected in LDA. The "Guidelines for the Management of Severe Traumatic Brain Injury" indicates the use of osmotic therapy for the treatment for intracranial hypertension after TBI[60]. While hypertonic solutions (i.e. hypertonic saline or mannitol) have been used extensively in an attempt to reduce intracranial pressure, recent sources suggest that reduction of ICP may not offer many significant benefits over isotonic solutions (particularly normal saline) and have associated concerns, such as increased infection risk[61-64]. Results from isotonic fluid therapy studies in TBI patients suggest that there is indeed a therapeutic benefit of isotonic fluid therapy in restoring blood pressure and volume without substantial risk of increasing ICP (a primary concern with hypotonic solutions administration). In this study, isotonic phosphate buffered saline (PBS) was used as vehicle, and we speculate that the acute systemic administration of a large volume of PBS (~4.8 mL over 48 hrs) to TBI rats may have contributed to tissue protection and the moderate improvement in behavioral recovery observed in vehicle treated animals, when compared to TBI control rats.

Increasing attention is being paid to the role of sex differences in TBI outcomes. Clinical studies reveal inconsistent results relating injury severity and mortality in the female population in comparison to age-matched males, and yet female populations are understudied in preclinical research[11,12,65]. Estrogen and progesterone can cross the blood-brain barrier, bind to hormone receptors widely expressed in the brain, and act as neuromodulators, reducing cell death and brain edema, and ultimately improving functional recovery in rodent TBI models[66]. Estrogen and progesterone have been reported to provide neuroprotection post-TBI, although a large clinical trial recently concluded that there was no clinical benefit to progesterone treatment after severe

TBI[16,66,67]. In our study, we sought to include age-matched females with consideration for hormone-mediated disparities in TBI prognosis and potential responses to NSC EV-based treatment. TBI inductions were therefore intentionally not matched to the estrous cycle of females. The large variations in immunohistochemical and behavioral response observed within the female population are likely due to hormonal and neuroendocrine changes that took effect during the time course of the assessment. In conclusion, male rats responded more sensitively to NSC EV treatment, while NSC EV treatment appeared to have variable effects on females. From these results, we infer that female hormones might introduce significant effects and that additional studies would be required to fully elucidate these effects in future preclinical studies.

In conclusion, acute intravenous injections of human NSC EVs increased the migration of endogenous NSCs to the lesion site and increased VEGF activity in male TBI rats, which promoted recovery of motor function. The therapeutic benefit of NSC EVs following TBI was significant in male rats, but variable in females. The potential role of female sex hormones in masking the therapeutic effects of NSC EVs should be considered in the design of future studies evaluating the preclinical and clinical potential of NSC EV therapy for TBI.

2.5 References

1 Centers for Disease, C. & Prevention. CDC grand rounds: reducing severe traumatic brain injury in the United States. *MMWR Morb Mortal Wkly Rep* **62**, 549-552 (2013).

2 Brooks, J. C., Shavelle, R. M., Strauss, D. J., Hammond, F. M. & Harrison-Felix, C. L. Long-Term Survival After Traumatic Brain Injury Part II: Life Expectancy. *Arch Phys Med Rehabil* **96**, 1000-1005, doi:10.1016/j.apmr.2015.02.002 (2015).

3 Loane, D. J. & Faden, A. I. Neuroprotection for traumatic brain injury: translational challenges and emerging therapeutic strategies. *Trends Pharmacol Sci* **31**, 596-604, doi:10.1016/j.tips.2010.09.005 (2010).

4 Reis, C. *et al.* Traumatic Brain Injury and Stem Cell: Pathophysiology and Update on Recent Treatment Modalities. *Stem Cells Int* **2017**, 6392592, doi:10.1155/2017/6392592 (2017).

5 Haus, D. L. *et al.* Transplantation of human neural stem cells restores cognition in an immunodeficient rodent model of traumatic brain injury. *Exp Neurol* **281**, 1-16, doi:10.1016/j.expneurol.2016.04.008 (2016).

6 Xiong, L. L. *et al.* Neural Stem Cell Transplantation Promotes Functional Recovery from Traumatic Brain Injury via Brain Derived Neurotrophic Factor-Mediated Neuroplasticity. *Mol Neurobiol* **55**, 2696-2711, doi:10.1007/s12035-017-0551-1 (2018).

7 Baraniak, P. R. & McDevitt, T. C. Stem cell paracrine actions and tissue regeneration. *Regenerative Medicine* **5**, 121-143, doi:10.2217/Rme.09.74 (2010).

8 Webb, R. L. *et al.* Human Neural Stem Cell Extracellular Vesicles Improve Recovery in a Porcine Model of Ischemic Stroke. *Stroke* **49**, 1248-1256, doi:10.1161/STROKEAHA.117.020353 (2018).

9 Webb, R. L. *et al.* Human Neural Stem Cell Extracellular Vesicles Improve Tissue and Functional Recovery in the Murine Thromboembolic Stroke Model. *Transl Stroke Res*, doi:10.1007/s12975-017-0599-2 (2017).

10 Lai, C. P. & Breakefield, X. O. Role of exosomes/microvesicles in the nervous system and use in emerging therapies. *Front Physiol* **3**, 228, doi:10.3389/fphys.2012.00228 (2012).

11 Slewa-Younan, S., Green, A. M., Baguley, I. J., Gurka, J. A. & Marosszeky, J. E. Sex differences in injury severity and outcome measures after traumatic brain injury. *Arch Phys Med Rehabil* **85**, 376-379 (2004).

12 Munivenkatappa, A., Agrawal, A., Shukla, D. P., Kumaraswamy, D. & Devi, B. I. Traumatic brain injury: Does gender influence outcomes? *Int J Crit Illn Inj Sci* **6**, 70-73, doi:10.4103/2229-5151.183024 (2016).

13 Vagnerova, K., Koerner, I. P. & Hurn, P. D. Gender and the injured brain. *Anesth Analg* **107**, 201-214, doi:10.1213/ane.0b013e31817326a5 (2008).

14 Caplan, H. W., Cox, C. S. & Bedi, S. S. Do Microglia Play a Role in Sex Differences in TBI? *Journal of Neuroscience Research* **95**, 509-517, doi:10.1002/jnr.23854 (2017).

15 Villapol, S., Loane, D. J. & Burns, M. P. Sexual dimorphism in the inflammatory response to traumatic brain injury. *Glia* **65**, 1423-1438, doi:10.1002/glia.23171 (2017).

16 Raghava, N., Das, B. C. & Ray, S. K. Neuroprotective effects of estrogen in CNS injuries: insights from animal models. *Neurosci Neuroecon* **6**, 15-29, doi:10.2147/NAN.S105134 (2017).

17 Liang, C. C., Park, A. Y. & Guan, J. L. In vitro scratch assay: a convenient and inexpensive method for analysis of cell migration in vitro. *Nat Protoc* **2**, 329-333, doi:10.1038/nprot.2007.30 (2007).

18 Al Sifri, S. *et al.* Prevalence of lipid abnormalities and cholesterol target value attainment in patients with stable coronary heart disease or an acute coronary syndrome in Saudi Arabia. *Saudi Med J* **39**, 697-704, doi:10.15537/smj.2018.7.22146 (2018).

19 Zhao, Z., Loane, D. J., Murray, M. G., 2nd, Stoica, B. A. & Faden, A. I. Comparing the predictive value of multiple cognitive, affective, and motor tasks after rodent traumatic brain injury. *J Neurotrauma* **29**, 2475-2489, doi:10.1089/neu.2012.2511 (2012).

20 Betancur, M. I. *et al.* Chondroitin Sulfate Glycosaminoglycan Matrices Promote Neural Stem Cell Maintenance and Neuroprotection Post-Traumatic Brain Injury. *ACS Biomater Sci Eng* **3**, 420-430, doi:10.1021/acsbiomaterials.6b00805 (2017).

21 Fonoff, E. T. *et al.* Functional mapping of the motor cortex of the rat using transdural electrical stimulation. *Behav Brain Res* **202**, 138-141, doi:10.1016/j.bbr.2009.03.018 (2009).

22 Karumbaiah, L. *et al.* Relationship between intracortical electrode design and chronic recording function. *Biomaterials* **34**, 8061-8074, doi:10.1016/j.biomaterials.2013.07.016 (2013).

23 Arribas, F. *et al.* Comments on the 2016 ESC Guidelines for the Management of Atrial Fibrillation. *Rev Esp Cardiol (Engl Ed)* **70**, 2-8, doi:10.1016/j.rec.2016.11.032 (2017).

24 Dixon, K. J. *et al.* Endogenous neural stem/progenitor cells stabilize the cortical microenvironment after traumatic brain injury. *J Neurotrauma* **32**, 753-764, doi:10.1089/neu.2014.3390 (2015).

25 Lever, J., Krzywinski, M. & Atman, N. POINTS OF SIGNIFICANCE Principal component analysis. *Nat Methods* **14**, 641-642, doi:DOI 10.1038/nmeth.4346 (2017).

26 Liu, L., Tang, L., Dong, W., Yao, S. & Zhou, W. An overview of topic modeling and its current applications in bioinformatics. *Springerplus* **5**, 1608, doi:10.1186/s40064-016-3252-8 (2016).

27 Yamashita, T., Takahashi, Y. & Takakura, Y. Possibility of Exosome-Based Therapeutics and Challenges in Production of Exosomes Eligible for Therapeutic Application. *Biol Pharm Bull* **41**, 835-842, doi:10.1248/bpb.b18-00133 (2018).

28 Gennai, S. *et al.* Cell-based therapy for traumatic brain injury. *Br J Anaesth* **115**, 203-212, doi:10.1093/bja/aev229 (2015).

29 Valadi, H. *et al.* Exosome-mediated transfer of mRNAs and microRNAs is a novel mechanism of genetic exchange between cells. *Nat Cell Biol* **9**, 654-659, doi:10.1038/ncb1596 (2007).

30 Reekmans, K. *et al.* Current challenges for the advancement of neural stem cell biology and transplantation research. *Stem Cell Rev* **8**, 262-278, doi:10.1007/s12015-011-9266-2 (2012).

31 Driscoll, D., Farnia, S., Kefalas, P. & Maziarz, R. T. Concise Review: The High Cost of High Tech Medicine: Planning Ahead for Market Access. *Stem Cells Transl Med* **6**, 1723-1729, doi:10.1002/sctm.16-0487 (2017).

32 Sutterlin, C. E., 3rd, Field, A., Ferrara, L. A., Freeman, A. L. & Phan, K. Range of motion, sacral screw and rod strain in long posterior spinal constructs: a biomechanical comparison between S2 alar iliac screws with traditional fixation strategies. *J Spine Surg* **2**, 266-276, doi:10.21037/jss.2016.11.01 (2016).

33 Zoerle, T. *et al.* Rethinking Neuroprotection in Severe Traumatic Brain Injury: Toward Bedside Neuroprotection. *Front Neurol* **8**, 354, doi:10.3389/fneur.2017.00354 (2017).

34 Hammell, C. L. & Henning, J. D. Prehospital management of severe traumatic brain injury. *BMJ* **338**, b1683, doi:10.1136/bmj.b1683 (2009).

35 Matsushima, K. *et al.* Emergent operation for isolated severe traumatic brain injury: Does time matter? *J Trauma Acute Care Surg* **79**, 838-842, doi:10.1097/TA.0000000000000719 (2015).

36 Kejriwal, R. & Civil, I. Time to definitive care for patients with moderate and severe traumatic brain injury--does a trauma system matter? *N Z Med J* **122**, 40-46 (2009).

37 Maghool, F., Khaksari, M. & Siahposht Khachki, A. Differences in brain edema and intracranial pressure following traumatic brain injury across the estrous cycle: involvement of female sex steroid hormones. *Brain Res* **1497**, 61-72, doi:10.1016/j.brainres.2012.12.014 (2013).

38 Wagner, A. K. *et al.* Evaluation of estrous cycle stage and gender on behavioral outcome after experimental traumatic brain injury. *Brain Res* **998**, 113-121 (2004).

39 Sofroniew, M. V. & Vinters, H. V. Astrocytes: biology and pathology. *Acta Neuropathol* **119**, 7-35, doi:10.1007/s00401-009-0619-8 (2010).

40 Anderson, M. A. *et al.* Astrocyte scar formation aids central nervous system axon regeneration. *Nature* **532**, 195-200, doi:10.1038/nature17623 (2016).

41 Burda, J. E., Bernstein, A. M. & Sofroniew, M. V. Astrocyte roles in traumatic brain injury. *Exp Neurol* **275 Pt 3**, 305-315, doi:10.1016/j.expneurol.2015.03.020 (2016).

42 Karumbaiah, L. *et al.* Relationship between intracortical electrode design and chronic recording function. *Biomaterials* **34**, 8061-8074, doi:10.1016/j.biomaterials.2013.07.016 (2013).

43 Villapol, S., Byrnes, K. R. & Symes, A. J. Temporal dynamics of cerebral blood flow, cortical damage, apoptosis, astrocyte-vasculature interaction and astrogliosis in the pericontusional region after traumatic brain injury. *Front Neurol* **5**, 82, doi:10.3389/fneur.2014.00082 (2014).

44 Erturk, A. *et al.* Interfering with the Chronic Immune Response Rescues Chronic Degeneration After Traumatic Brain Injury. *J Neurosci* **36**, 9962-9975, doi:10.1523/JNEUROSCI.1898-15.2016 (2016).

45 Rabinowicz, T. *et al.* Structure of the cerebral cortex in men and women. *J Neuropathol Exp Neurol* **61**, 46-57 (2002).

46 Acaz-Fonseca, E., Duran, J. C., Carrero, P., Garcia-Segura, L. M. & Arevalo, M. A. Sex differences in glia reactivity after cortical brain injury. *Glia* **63**, 1966-1981, doi:10.1002/glia.22867 (2015).

47 Sung, B. H., Ketova, T., Hoshino, D., Zijlstra, A. & Weaver, A. M. Directional cell movement through tissues is controlled by exosome secretion. *Nat Commun* **6**, 7164, doi:10.1038/ncomms8164 (2015).

48 Shabbir, A., Cox, A., Rodriguez-Menocal, L., Salgado, M. & Van Badiavas, E. Mesenchymal Stem Cell Exosomes Induce Proliferation and Migration of Normal and Chronic Wound Fibroblasts, and Enhance Angiogenesis In Vitro. *Stem Cells Dev* **24**, 1635-1647, doi:10.1089/scd.2014.0316 (2015).

49 Webb, D. J., Parsons, J. T. & Horwitz, A. F. Adhesion assembly, disassembly and turnover in migrating cells -- over and over and over again. *Nat Cell Biol* **4**, E97-100, doi:10.1038/ncb0402-e97 (2002).

50 Chang, E. H. *et al.* Traumatic Brain Injury Activation of the Adult Subventricular Zone Neurogenic Niche. *Front Neurosci* **10**, 332, doi:10.3389/fnins.2016.00332 (2016).

51 Webb, R. L. *et al.* Human Neural Stem Cell Extracellular Vesicles Improve Tissue and Functional Recovery in the Murine Thromboembolic Stroke Model. *Transl Stroke Res* **9**, 530-539, doi:10.1007/s12975-017-0599-2 (2018).

52 Addington, C. P., Roussas, A., Dutta, D. & Stabenfeldt, S. E. Endogenous repair signaling after brain injury and complementary bioengineering approaches to enhance neural regeneration. *Biomark Insights* **10**, 43-60, doi:10.4137/BMI.S20062 (2015).

53 Xin, H. *et al.* Exosome-mediated transfer of miR-133b from multipotent mesenchymal stromal cells to neural cells contributes to neurite outgrowth. *Stem Cells* **30**, 1556-1564, doi:10.1002/stem.1129 (2012).

54 Nowacka, M. M. & Obuchowicz, E. Vascular endothelial growth factor (VEGF) and its role in the central nervous system: a new element in the neurotrophic hypothesis of antidepressant drug action. *Neuropeptides* **46**, 1-10, doi:10.1016/j.npep.2011.05.005 (2012).

55 Wittko-Schneider, I. M., Schneider, F. T. & Plate, K. H. Brain homeostasis: VEGF receptor 1 and 2-two unequal brothers in mind. *Cell Mol Life Sci* **70**, 1705-1725, doi:10.1007/s00018-013-1279-3 (2013).

56 Skold, M. K., von Gertten, C., Sandberg-Nordqvist, A. C., Mathiesen, T. & Holmin, S. VEGF and VEGF receptor expression after experimental brain contusion in rat. *J Neurotrauma* **22**, 353-367, doi:10.1089/neu.2005.22.353 (2005).

57 Lee, C. & Agoston, D. V. Vascular Endothelial Growth Factor Is Involved in Mediating Increased De Novo Hippocampal Neurogenesis in Response to Traumatic Brain Injury. *J Neurotraum* **27**, 541-553, doi:10.1089/neu.2009.0905 (2010).

58 Ma, Y., Zechariah, A., Qu, Y. & Hermann, D. M. Effects of vascular endothelial growth factor in ischemic stroke. *J Neurosci Res* **90**, 1873-1882, doi:10.1002/jnr.23088 (2012).

59 Harting, M. T. *et al.* Cell therapies for traumatic brain injury. *Neurosurg Focus* **24**, E18, doi:10.3171/FOC/2008/24/3-4/E17 (2008).

60 Haddad, S. H. & Arabi, Y. M. Critical care management of severe traumatic brain injury in adults. *Scand J Trauma Resusc Emerg Med* **20**, 12, doi:10.1186/1757-7241-20-12 (2012).

61 Bhatoe, H. S. Intravenous Fluids in Head Injury. *Indian J Neurotraum* **2**, 1-2 (2005).

62 Zornow, M. H. & Prough, D. S. Fluid management in patients with traumatic brain injury. *New Horiz* **3**, 488-498 (1995).

63 Qureshi, A. I., Suarez, J. I., Castro, A. & Bhardwaj, A. Use of hypertonic saline/acetate infusion in treatment of cerebral edema in patients with head trauma: Experience at a single center. *J Trauma* **47**, 659-665, doi:Doi 10.1097/00005373-199910000-00009 (1999).

64 Coritsidis, G. *et al.* Hypertonic saline infusion in traumatic brain injury increases the incidence of pulmonary infection. *J Clin Neurosci* **22**, 1332-1337, doi:10.1016/j.jocn.2015.02.025 (2015).

65 Wright, D. W. *et al.* Gender differences in neurological emergencies part II: a consensus summary and research agenda on traumatic brain injury. *Acad Emerg Med* **21**, 1414-1420, doi:10.1111/acem.12532 (2014).

66 Brotfain, E. *et al.* Neuroprotection by Estrogen and Progesterone in Traumatic Brain Injury and Spinal Cord Injury. *Curr Neuropharmacol* **14**, 641-653 (2016).

67 Wei, J. & Xiao, G. M. The neuroprotective effects of progesterone on traumatic brain injury: current status and future prospects. *Acta Pharmacol Sin* **34**, 1485-1490, doi:10.1038/aps.2013.160 (2013).

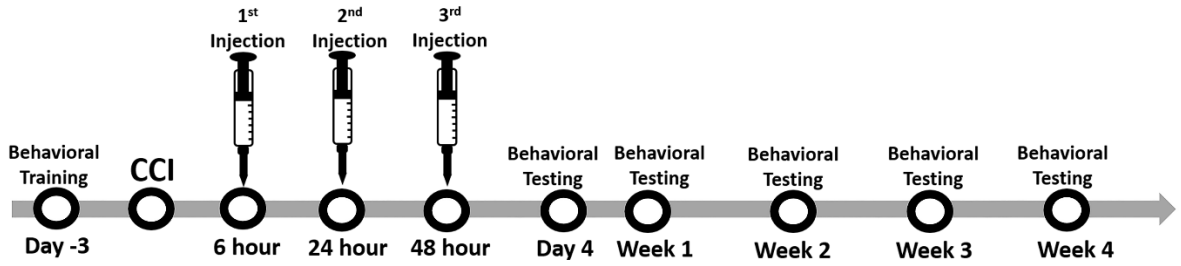

Figure 2.1 Experimental schedule. Animals were pre-trained on the beam-walk test prior to CCI induction. Following behavioral pre-training, a left hind limb deficit was induced via CCI to the rat motor cortex. Animals were randomly assigned to one of the following treatment groups: NSC EV, vehicle, or TBI control. Three doses of NSC EV (4e10 EVs/kg) or vehicle at 6 hr, 24 hr, and 48 hr post-CCI were injected via tail vein. No injections were administered to the TBI control rats following CCI. Behavioral assessment was performed on 4, 7, 14, 21 and 28 days post-CCI.

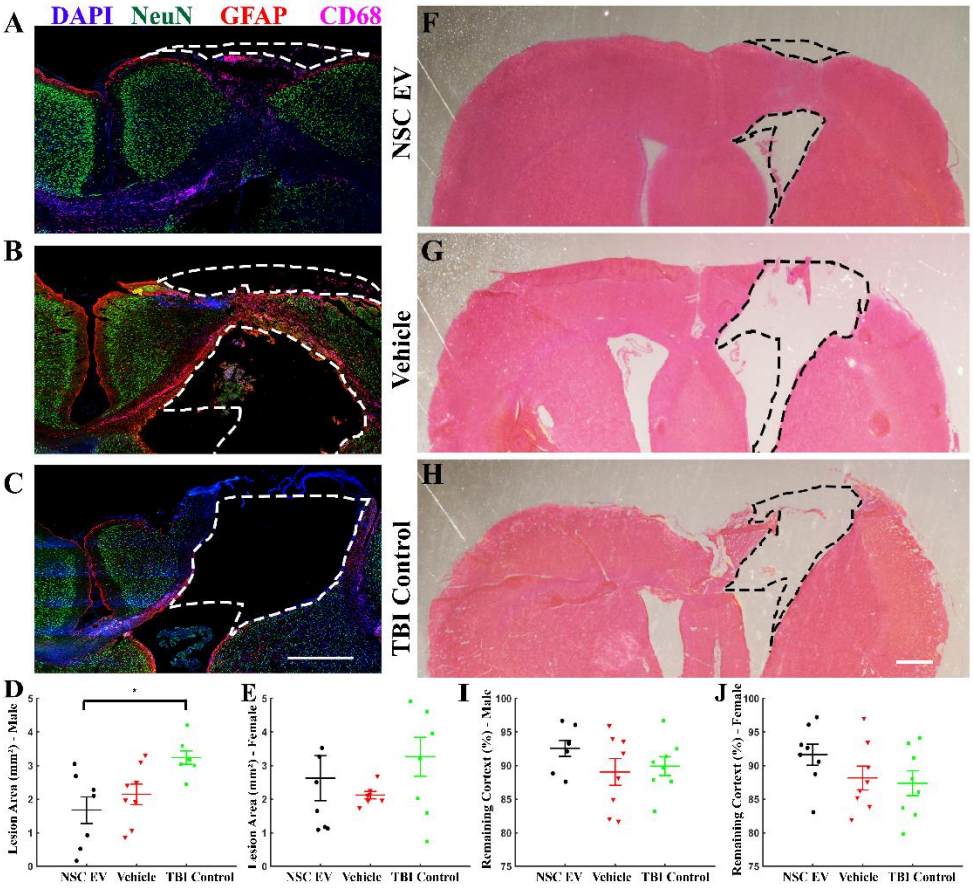

Figure 2.2 Acute intravenous administration of NSC EVs reduced tissue loss in male TBI rats. Contralateral hemisphere was overlaid to the injured hemisphere to outline the lesion and to estimate the volume of tissue lost. Representative images of A) male NSC EV-treated, B) male vehicle-treated, and C) male control brain tissue stained for neurons (NeuN; green), reactive astrocytes (GFAP; red), macrophages and microglia (CD68; magenta) and DAPI counterstain (blue). Scale bar = 1 mm. D, E) NSC EV-treated rats demonstrated a significant decrease in lost tissue compared to TBI control rats in males; females showed a similar, although non-significant, trend to males. Representative H&E stained images of F) male NSC EV-treated, G) male vehicle-treated, and H) male control brain tissue. Scale bar = 500 μm. I, J) NSC EV-treated rats demonstrated a marginal increase in preserved tissue compared to vehicle-treated or TBI control rats in both males and females. *P<0.05.

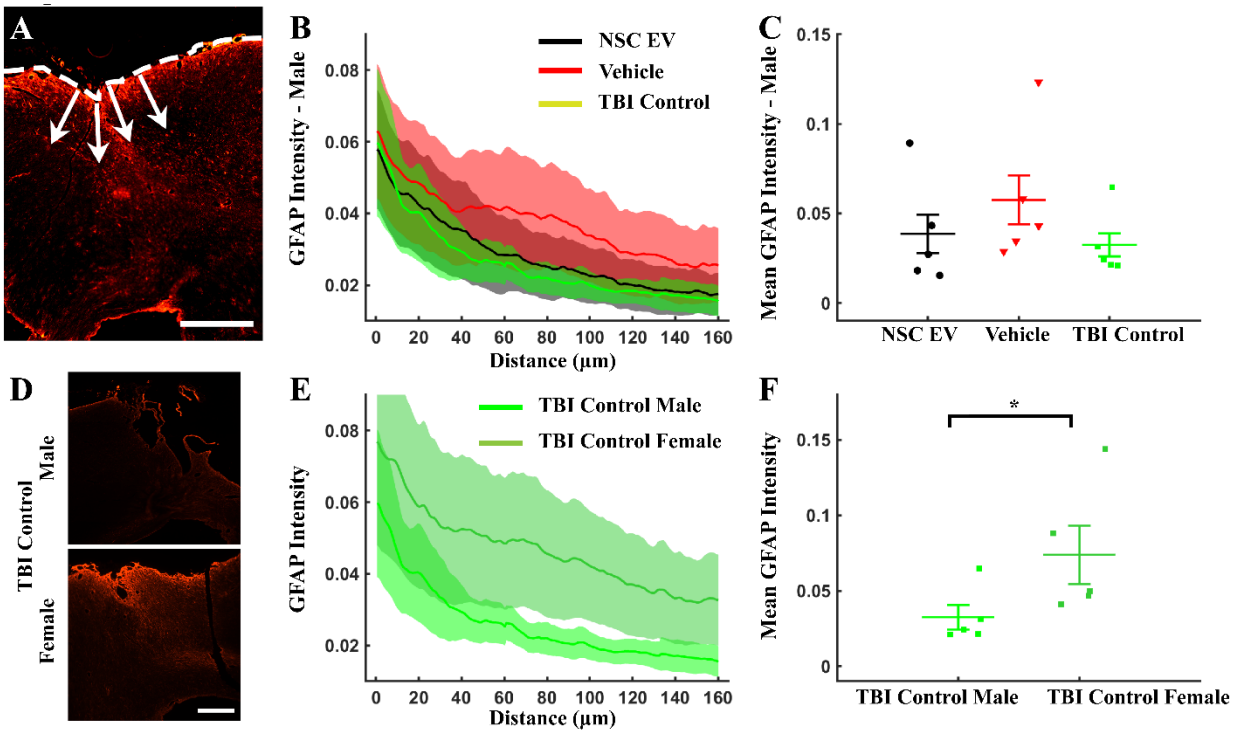

Figure 2.3 NSC EV treatment did not affect local GFAP expression. A) Fluorescence intensity values were obtained along lines (arrows) drawn perpendicularly to the lesion (dashed line) and to a distance of 160 µm away from the lesion site. Scale bar = 500 µm. B) The GFAP intensity values from the impact site (0 µm) to 160 µm away from the center of the injury demonstrated decreasing expression of GFAP in male groups. C) Mean intensity in the perilesional area showed no significant differences in GFAP intensity across three treatment groups in male rats. D) Representative images of male TBI control (upper) and female TBI control (lower) GFAP staining showing difference in intensity. Scale bar = 200 µm. E,F) The mean intensity in the perilesional GFAP response following TBI was lower over the entire depth in control male compared to control female indicating intrinsic gender differences. *P<0.05.

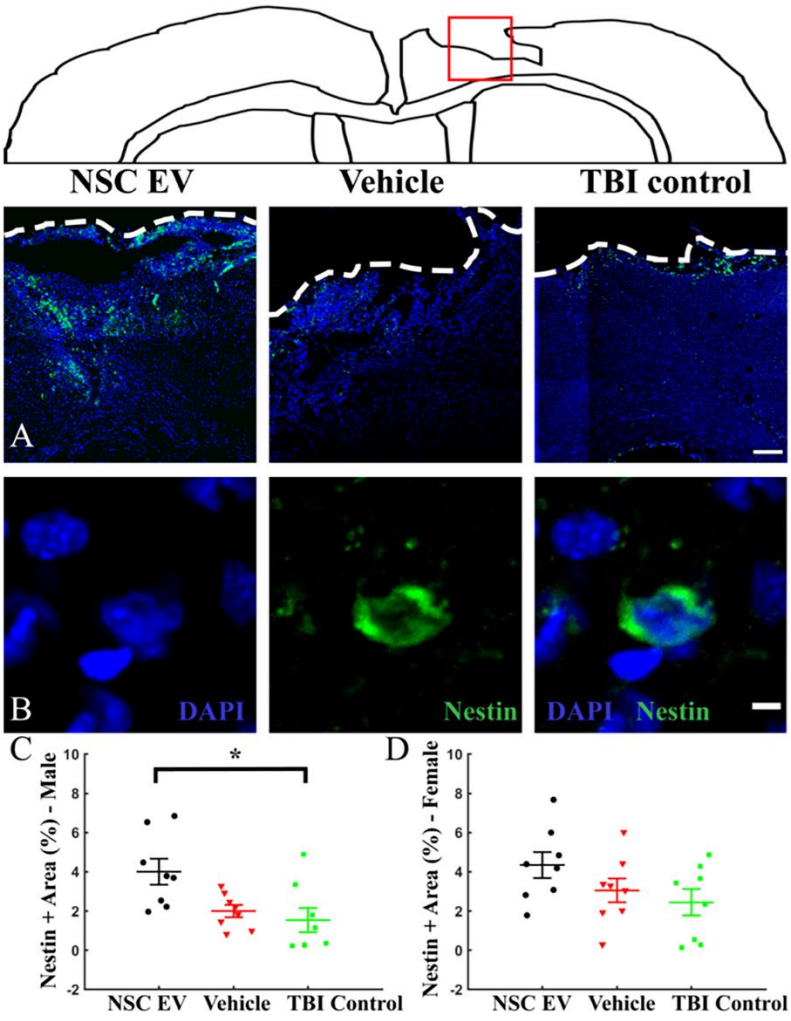

Figure 2.4 Endogenous NSC presence was significantly enhanced by NSC EV treatment. Representative coronal brain section images corresponding to the red box surrounding the lesion area stained for A) nestin (green) merged with DAPI counterstain (blue). White dashes outline injury penumbra. Scale bar = 250 μm. B) Nestin staining at a higher magnification. Scale bar = 5 μm. C) Quantification of the mean nestin expression over tissue area at the site of the injury revealed significantly increased nestin expression in NSC EV-treated male rats when compared to the TBI control males and a strongly trending increase over vehicle-treated males. D) A similar trend was observed in female rats. *$p<0.05$.

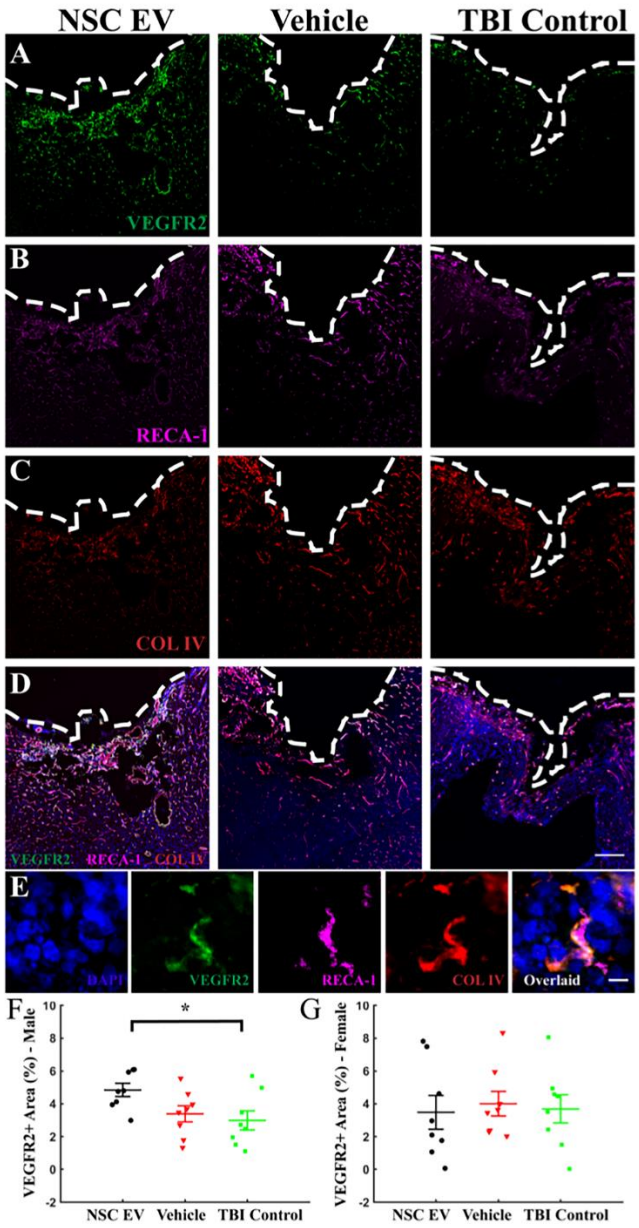

Figure 2.5 VEGFR2 (Flk-1) staining showed an increased local VEGF activity in NSC EV-treated male rats. Representative images of A) VEGFR2 (green), B) RECA-1 (magenta) and C) COL IV (red) from each male treatment group. D) All channels overlaid and counterstained with DAPI (blue). Scale bar = 250 μm. E) At a higher magnification. Scale bar = 10 μm. F) Enhanced local expression of VEGFR2 was observed in male NSC EV-treated rats, while G) female rats showed no significant difference. *$p<0.05$.

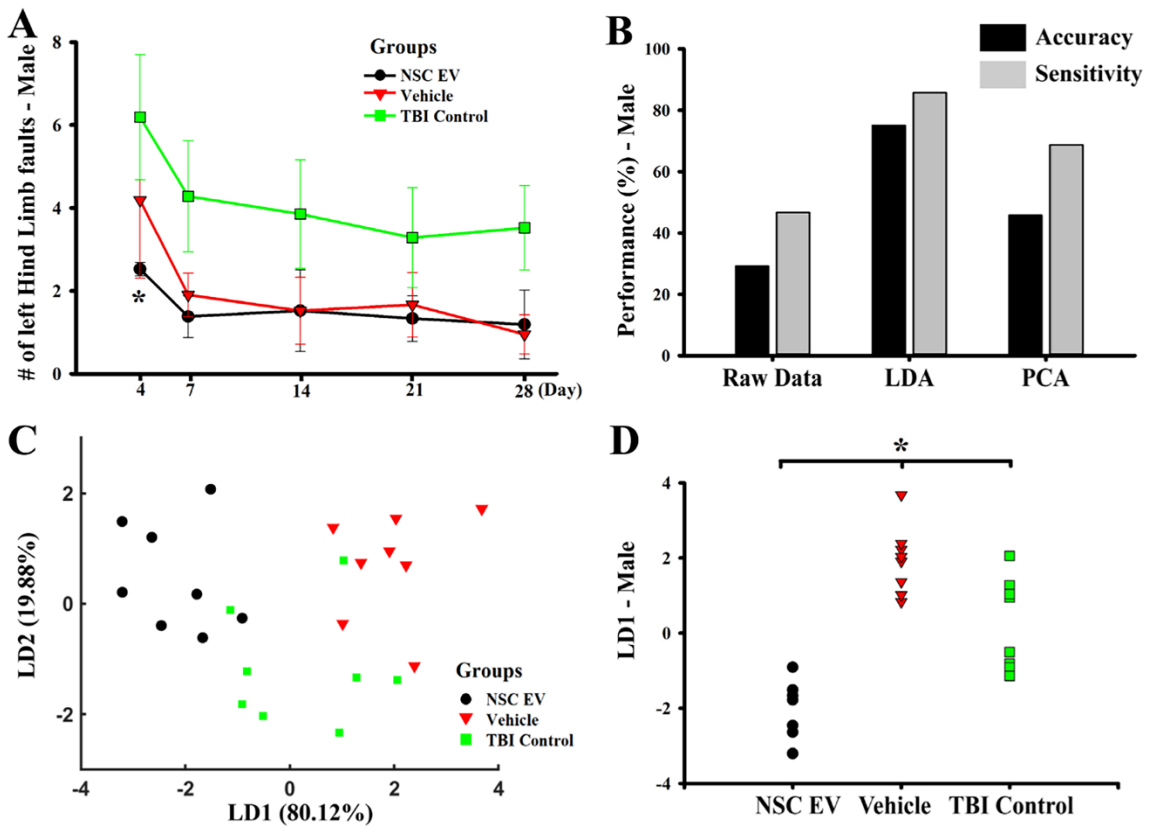

Figure 2.6 NSC EV-treatment significantly improved behavioral and global indexes of recovery in TBI males. A) NSC EV-treated male rats subjected to a beam walk test exhibited motor function recovery. At day 4, NSC EV-treated males exhibited significantly reduced motor balance deficit when compared to the TBI control, but not to vehicle-only controls. B) Performance of a linear Fisher classification using raw data (11 variables), LDA dimensionality reduction (2 first components with highest explained variance) and PCA dimensionality reduction (2 first principal components with highest explained variance). LDA-based classification outperformed raw data and PCA. C) Significant separation was observed between male NSC EV-treated, vehicle-treated and TBI control rats using LDA composite scores (dimensionality reduction). D) Group separation using LD1 revealed significance. *$p<0.05$. LDA: linear discriminant analysis; PCA: principal component analysis.

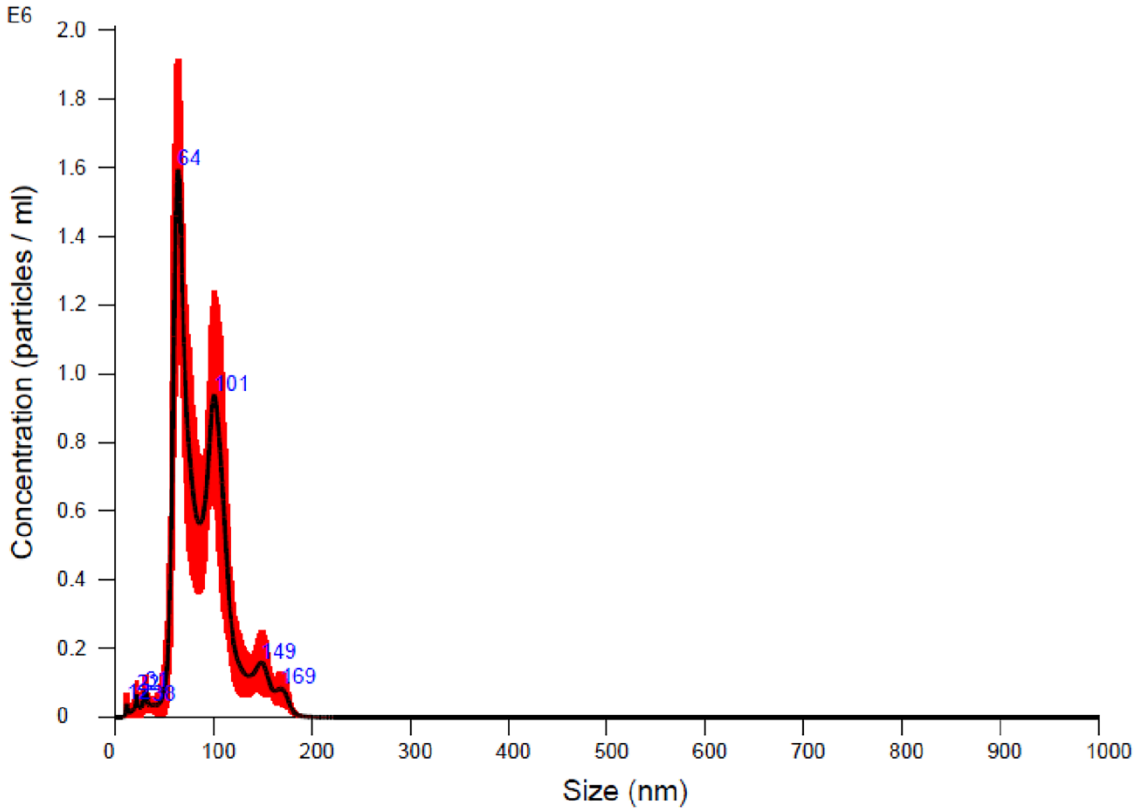

Supplementary Figure 2.1 Nanoparticle tracking analysis (NTA) of NSC EVs indicates an average size distribution of ~64-100 nm in diameter.

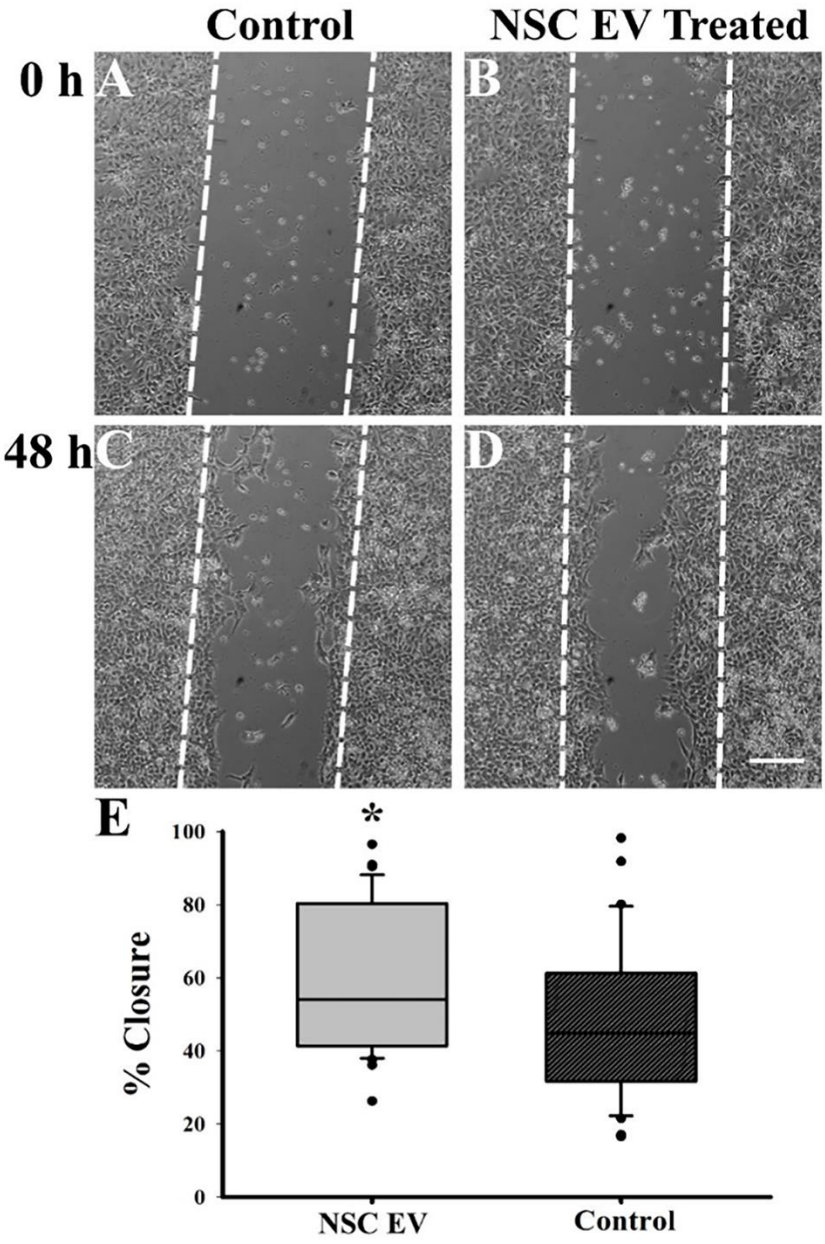

Supplementary Figure 2.2 *In vitro* scratch wound assay demonstrating the NSC EV-induced enhancement in NSC migration. Representative bright field images of A) untreated control and B) NSC EV-supplemented NSCs at time 0; and C) control and D) NSC EV-supplemented NSCs after 48 hours. Scale bar= 200 μm. E) The average percentage of closure of the scratched surface by NSCs was significantly increased with NSC EV treatment in comparison to the control NSCs with standard cell culture media. *$p<0.05$.

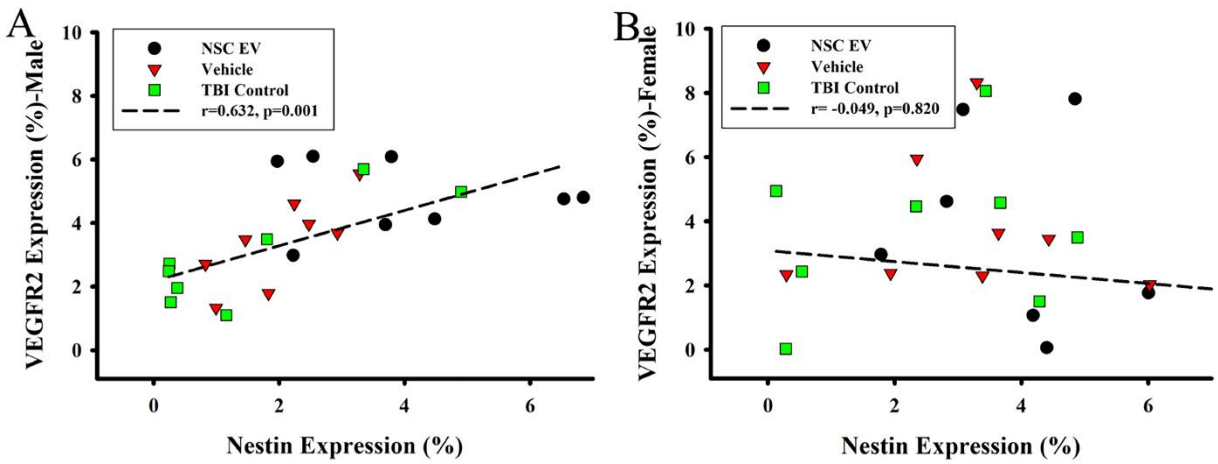

Supplementary Figure 2.3 Nestin and VEGFR2 expression showed an association in male rats. The scatter plot represents individual animals. A) A positive linear correlation was observed in male rats between nestin and VEGFR2 expression. B) Female rats did not exhibit correlation.

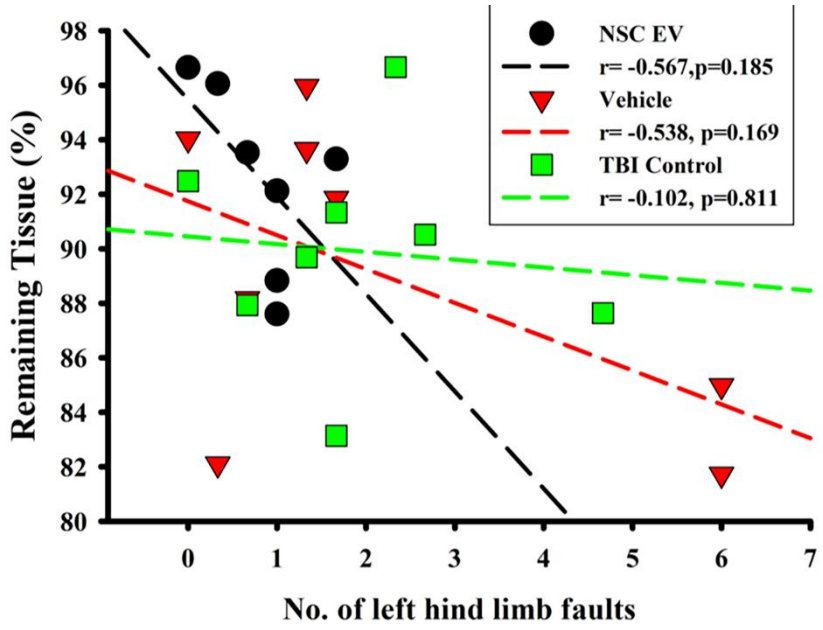

Supplementary Figure 2.4 Correlation between the remaining tissue percentage and the number of left hind limb faults. An overall negative association was observed in males, although non-significant.

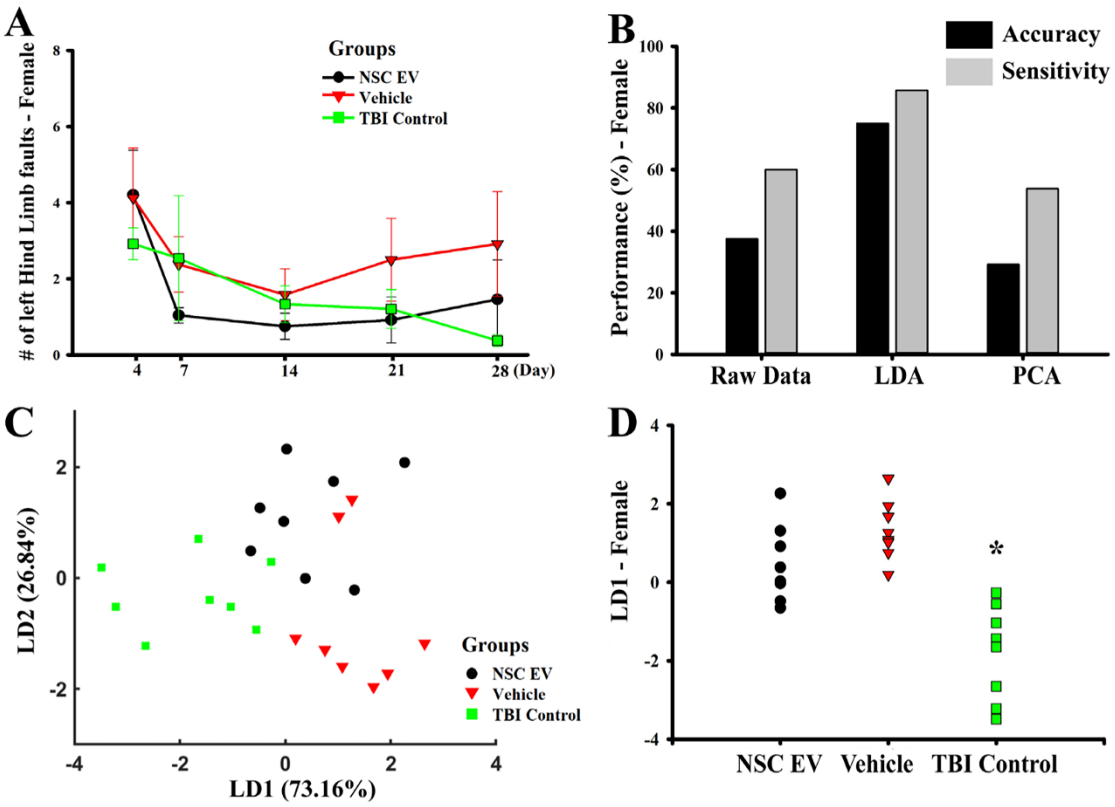

Supplementary Figure 2.5 NSC EV-treatment marginally improved recovery in TBI females. A) NSC EV-treated female rats subjected to a beam walk test exhibited overall motor function recovery over 4 weeks post-CCI, although no significant difference was found compared to vehicle-treated and control TBI females. B) Performance of linear Fisher classification using raw data (11 variables), LDA dimensionality reduction (2 first components with highest explained variance) and PCA dimensionality reduction (2 first principal components with highest explained variance). LDA-based classification outperformed raw data and PCA in females as in males. C) Separation was observed between NSC EV-treated, and TBI control female rats using LDA components, with some overlap with vehicle-treated female rats. D) Group separation using LD1 revealed significant separation of NSC EV-treated and vehicle-treated rats from TBI control rats. *$p<0.05$.

CHAPTER 3

SULFATION-MODIFIED CHONDROITIN SULFATE "CLICK" HYDROGELS SUPPORT HNSC MAINTNANCE AND NEURONAL ACTIVITY IN VITRO[2]

[2] Sun, M. K., Chopra, P., Latchoumane, C., Hudlikar, M.S., Boons, G., Karumbaiah, L. To be submitted to *Carbohydrate Polymers*.

Abstract

Chondroitin sulfate (CS) displaying a diverse array of sulfated residues is an integral constituent of the germinal stem cell niche in the mammalian brain, where they regulate stem cell function and neurogenesis. We hypothesized that sulfation-modified CS polymers that are functionalized with a cell adhesion promoting fusion peptide will enhance the proliferation and migration of human neural stem cells (hNSCs) and support neuronal activity of differentiated neurons. We encapsulated hNSCs in 3D hydrogels that were composed of unmodified or regioselectively sulfonated CS polymers with a cell adhesion promoting fusion peptide, using strain-promoted alkyne-azide cycloaddition (SPAAC) "click" chemistry. Our results demonstrated that hNSCs encapsulated in disulfated CS-4,6 disaccharide rich hydrogel displayed greater proliferation, formed larger aggregates, and increased migration when compared to those encapsulated in monosulfated hydrogels composed predominantly of CS-4 sulfate. Both scaffolds supported neuronal activity of differentiated neurons as detected by calcium imaging, however, neuritogenesis was encouraged in CS-4 sulfate rich hydrogel. Overall, these studies demonstrate the utility of sulfation-modified CS scaffolds as physiologically relevant microenvironments for investigating hNSC function in vitro.

Keywords: chondroitin sulfate, hydrogel, click chemistry, neural stem cells, sulfation

3.1 Introduction

The brain extracellular matrix (ECM) provides structural support to the neuronal network, and constitutes approximately one-fifth of the total brain volume[1]. One of the most distinctive features of the brain ECM is relatively low content of fibrous matrix proteins such as collagens, fibronectin and vitronectin, and basement membrane proteins, laminin, while higher presence of proteoglycans is observed[2]. Fibrous proteins provide structural support and present a nanofibrous topography, and the basement membrane proteins play an important role in cell adhesion and mediate cellular response via integrin binding[3]. Proteoglycan consists of a core protein and a glycosaminoglycan (GAG) moiety. In addition to providing structural stability, proteoglycans are involved in various cellular bio-active functions[4,5]. In this study, we pay a special attention to chondroitin sulfate (CS) not only because it is the most abundant GAG in the brain ECM, representing about 20% of its volume[6], but also due to its ability to interact with multiple growth factors, either specifically or non-specifically owing to its negatively charged electrostatic force[5].

The epimerization and sulfation patterns result in different forms of CS, namely chondroitin-4-*O*-sulfate (CS-A), chondroitin-6-*O*-sulfate (CS-C), chondroitin-2,6-di-*O*-sulfate (CS-D) and chodroitin-4,6-di-*O*-sulfate (CS-E) bearing variant negative charges[7]. The presentation of various CSs within the brain are tightly regulated spatio-temporally [4], as CS interacts with basic amino acid residues in positively charged growth factors to modulate release and binding of these growth factors to the neighboring cells[8]. CS-A composites approximately 80-90% of the brain CSs, demonstrating higher presence in the perineural network of the cortex[9,10]. Although CS-E is present in a lesser quantity (<5% of total CS)[10], it plays a critical role in growth factor binding due to its strong electrostatic attraction to binding partners[11].

Multiple studies have demonstrated that CS-E has a high binding affinity to fibroblast growth factors (FGF), midkine (MK), pleiotrophin (PTN), and more[12,13]. The ability to sequester and retain multiple growth factors and neurotrophic factors makes CS an attractive candidate for creating a brain mimetic *in vitro*.

Moreover, growing evidence points to sulfate groups of the CS providing specific binding domains. Using a synthetic glycan microarray approach, Gama et.al demonstrated that the binding of sulfated CS to proteins is dependent on the "sulfation code", or the specific sulfation pattern and not solely on electrostatic effects[14]. Although CS-E and CS-D have the same number of sulfate groups, CS-E displayed higher affinity to growth factors including brain-derived neurotrophic factor (BDNF), netrin1, slit2, ephrinA1 and semaphorin5B, which have strong implications in neuronal growth and axonal guidance[15]. CS-E is also proposed as a binding partner or a co-receptor for multiple heparin-binding growth factors, including FGF2[13], and the activation of the MAPKinase pathway in NSCs via FGF2 requires CS[16]. More recent studies revealed the presence of CSPG binding receptors on neuronal cell surfaces that are related to neurite outgrowth inhibition: nogo receptor family members (NgR1, NgR3), protein tyrosine phosphatase (PTPσ), and leukocyte common antigen-related receptors (LAR)[17,18].

In this study, CS hydrogel is crosslinked and modified via copper-free "click" chemistry to study the sulfation dependent effect of CS on hNSC proliferation, migration, and network function. The degree of sulfation was modulated by increasing the ratio of CS-E to CS-A. Mechanical properties were characterized via scanning electron microscopy (SEM), rheology, along with the swelling and degradation ratio. Proliferation of hNSCs encapsulated in either CS-A or CS-E rich hydrogels was determined based on 5-ethynyl-2′-deoxyuridine (EdU) incorporation. Activated hNSCs in CS hydrogels as determined by the sox1 staining was used to

support the proliferation data. hNSC migratory speed and focal adhesion sites (focal adhesion kinase/vinculin stain) were examined, as well as aggregation pattern, to address the possible mechanism for enhanced proliferation in CS-E rich hydrogels. Additionally, neuronal network functionality, as well as the morphogenesis, was assessed in CS hydrogels utilizing calcium imaging (fluo-4 AM), and class III β-tubulin (B3T) staining to demonstrate the versatile application of CS hydrogels within the central nervous system (CNS).

3.2 Results and Discussion

3.2.1 Chemical synthesis. Strain promoted azide-alkyne cycloaddition (SPAAC) reaction offers a rapid, facile, and biocompatible method for hydrogel fabrication. Unlike photo-crosslinking approaches[19], it does not require a catalyst and produces no byproducts. It is highly regioselective, which guarantees protection to encapsulated cells or the tissue (at site of transplantation) from unwanted chemical modifications or reactions[20]. To prepare CS hydrogels via click reaction (Figure 1), we synthesized an azide-functionalized CS-A (6) and CS-E (7), to cross link with a dibezocyclooctyne (DIBO) functionalized CS-A (8). To avoid any steric issues, we choose a small ethylene glycol linker (1) to modify CS backbone. By stochiometric control, one amine group of 1 was modified with either azide [21] or DIBO (3) leaving another amine group free for conjugation (Figure 1A). The amine group of the linker (2 or 3) was coupled to the carboxylic acid group of GlcA of CS-A (4) or CS-E (5) using carbodiimide chemistry to afford 6 (from 4), 7 (from 5) and 8 (from 4) in high yields (Figure 1B). The efficiency of coupling and degree of functionalization was determined using 1D/2D nuclear magnetic resonance (NMR) experiments. A stack plot of ^{1}H NMR spectra of 2, 4 and 6 (Figure 1C) and 3, 4 and 8 (Figure 1D) highlights characteristic peaks. Acceptable level of functionalization was observed, 35-45% for 6 (or 7) and 10-15% for 8. In

addition, an azide-modified fusion peptide was incorporated to promote adhesion, because CS is known to inhibit cell adhesion and spreading *in vitro*[22]. Without the presence of glycoproteins and fibrous proteins, which plays a large role in initiating cell adhesion and growth cone spreading *in vivo*[23], CS alone is insufficient to support cell adhesion. The inhibition of cell attachment by CS is not attributed to the non-specific masking of the adhesion proteins, and adhesion promoted by laminin is less effected by the presence of CS, in comparison to the adhesion promoted by fibronectins and vitronectins[24]. Hence, bioactive fusion peptide including laminin-derived motifs[25] was chosen in this study to aid cell adhesion in CS hydrogels.

3.2.2 Preparation and characterization of CS click hydrogels. In order to test crosslinking efficacy of CS hydrogel components (6-8), 2.5% of 6 (or 7) was mixed with 1% of 8 in a glass vial and incubated at room temperature. A stable hydrogel was formed within 10 minutes, as judged by vial-tilting method.

To confirm biocompatibility of the crosslinked hydrogel, mechanical properties were examined prior to cell encapsulation (Figure 2). CS hydrogels with 3.5% and 3% total CS concentrations were subjected to physio-mechanical testing based on the previous study[26]. Lyophilized hydrogels were imaged using scanning electron microscopy (SEM; Figure 2A, B). 3.5% CS hydrogel displayed a denser structural network with 17.2±12.0 μm measured average pore size (diameter), while 3% CS hydrogel has larger pore size of 25.2±17.5 μm. Next, CS hydrogels were tested for their rheological properties (Figure 2C). The storage modulus of the 3.5% CS hydrogel ranged between 400 and 1000Pa as the frequency sweep increased, while 3% CS hydrogel's storage modulus remained relatively low, barely reaching 400 Pa at 100 rad/s. 3.5% CS hydrogel was selected optimal for cell culture as displays storage modulus akin to human brain tissue (600-1100 Pa)[27]. We tested swelling and degradation properties of 3.5% CS hydrogels over

a period of 14 days both in the presence an absence of hyaluronidase (Figure 2D). Swelling ratio was 87.91±3.43%, and degradation ratio was 81.28±1.18% at the end of 14 days. In summary, we investigated pore size, stiffness and degradation time of CS hydrogels to meet the physical features of brain tissue. The CS gels displays physical and mechanical properties to ensure diffusion of nutrients and oxygen, cell migration/adhesion and cell survival[28]. Studies have shown that bio-scaffold alone can induce regeneration in injured brains, which underscore the importance of the material design including mechanical elements[29]. Indeed, viability of the human induced pluripotent neural stem cell (hNSC) encapsulated in 3.5% CS hydrogel was largely unaffected (Supplementary Figure 1; 81.6±12.1%).

3.2.3 CS-E rich hydrogel enhances hNSC proliferation. We hypothesized that CS hydrogel rich in CS-E would encourage hNSC proliferation owing to its interaction with FGF-2, and its potential role as a FGF-2 reservoir to assist binding of FGF-2 to the cell surface[13]. For the CS-E rich hydrogel, commercially available CS-A (~80% CS-A containing other forms of CS) was subjecte do chemical *O*-sulfation to afford a CS mixture with ~50% CS-E[30]. The 6-*O*-sulfation of GalNAc residue was confirmed by ^{1}H NMR and ^{1}H-^{13}C heteronuclear single quantum coherence spectroscopy (HSQC, 2D-NMR), which shows a distinct downfield shift of ring carbon C-6 and proton H-6 (Figure 1). The CS-E obtained was further coupled to azide linker (Figure 1B, 2) to obtain azido-functionalized CS-E (Figure 1B, 7). Final CS compositions of CS-A and CS-E rich hydrogels are shown in Table 1. hNSCs encapsulated CS-A and CS-E rich hydrogels were subjected to the 5-ethynyl-2'-deoxyuridine (EdU) proliferation assay (Figure 3). EdU was incorporated into the newly synthesized DNA, hence tagging proliferating hNSCs during the time of incubation (3 hrs). Flow cytometry revealed 22.7% of the hNSCs encapsulated in CS-E rich hydrogel went through S phase during the 3 hr time window, which is significantly higher than the

proliferation rate of hNSCs in CS-A rich hydrogel (20.1%; chi-square, $p<0.001$). Next, hNSCs were stained with the activated stem marker, sox1[31], to determine if the difference observed in proliferation was due to heterogeneous hNSC population[32] (Figure 4H, I, J). No difference (Mann-Whitney Rank Sum, $p=0.178$) was observed between sox1 expressing cells in CS-A hydrogel compared to CS-E hydrogel, with the majority of the cells staining positive for sox1.

Adult hNSCs in the ventricle-subventricular zones have a S phase length between 4-9 hrs[33]. Results indicate that although most hNSCs encapsulated in both CS-A and C-E rich hydrogels were in their activated states, hNSCs in CS-E rich hydrogel increased the rate of proliferation. FGF-2 is required for hNSC proliferation, and failure to either produce FGF-2 *in vivo*[34,35] or supplement FGF-2 *in vitro*[36] will stunt neurogenesis. Presence of CS is critical for FGF-2 dependent proliferation as CS is required for the activation of downstream pathways[16]. Evidence suggests that highly sulfated CS binds to FGF-2 with high affinity which in turn, activates FGF-2 dependent mitogenic responses[37,38]. FGF-2 degrades rapidly in culture medium and the presence of NSCs enhances the reat of degradation, only 50% remaining after 48 hrs[39]. We speculate CS-E rich hydrogel efficiently binds to FGF-2 in culture and retains its functional integrity FGF-2 in culture to prolong the activation of FGF-2 dependent proliferation in hNSCs.

3.2.4 CS-E rich hydrogel increases hNSC migration and aggregation. To further investigate the potential contributing factor to enhanced hNSC proliferation in CS-E rich hydrogel, hNSC migration speed in CS-A and CS-E rich hydrogel was calculated via live-cell imaging (Figure 4). 10 minutes post-encapsulation, Hoechst and DiO labelled hNSCs were imaged for 30 minutes to measure their migration trajectories and the average speed was calculated. The average speed of hNSCs in CS-E hydrogel (54.546±7.109 μm/hr) was significantly increased (Mann-Whitney Rank Sum, $p=0.05$) compared to the hNSCs in CS-A hydrogel (58.334±5.804μm/h). hNSC migration

speed greater than 30μm/h was categorized as a cell with high migratory potential. hNSCs in CS-A and CS-E rich hydrogels were binned into either high or low migratory potential cells (Figure 5B): CS-E rich hydrogel (64.9%) had almost twice as many cells with high migratory potential than CS-A rich hydrogel (35.1%; chi-square: $p<0.001$). Since an increased number of focal adhesions indicates enhanced migration[40], the number of focal adhesions (FAK/vinculin colocalization) per cell was examined upon crosslinking (Figure 5C,D,E). In accordance with the migration speed, hNSCs in CS-E rich hydrogel (median=1.906) expressed higher number of focal adhesions than hNSCs in CS-A rich hydrogel on average (median=0.933; Mann-Whitney Rank Sum, $p=0.034$). At 48-hour post-encapsulation, hNSCs were stained with the stem cell cytoskeletal marker, nestin, to study how hNSCs were distributed within the hydrogel after immediate migration (Figure 6). We observed that hNSCs formed larger aggregates in CS-E rich hydrogel (median=64.474; Mann-Whitney Rank Sum, $p<0.001$) with 30.8% of the aggregate area larger than 100 μm^2, while 12.5% of the aggregates were larger than 100 μm^2 (chi-square, $p<0.001$) in CS-A rich hydrogel (median=50.362).

Interestingly, our data suggests that CS-E rich hydrogel promotes migration of encapsulated hNSCs to form larger spheroids/aggregates. One of the major factors that guide NSC spreading, and migration is the mechanics of the microenvironment. The activation of mechano-transducers via ECM rigidity and topography are well-demonstrated[41]. Through characterization, we have demonstrated that both CS-A and CS-E rich hydrogels are comparable to the naïve brain ECM and minimal difference exists between two hydrogels. Another factor influencing NSC migration is chemical cue via integrin binding[42]. Chondroitin sulfate has shown to limit NSC motility/migration through ROCK activation *in vitro*[43], however, *in vivo* data suggests an opposing view. In the developing neocortex, depletion of over sulfated CS led to impaired radial migration

of the neural progenitor cells by preventing NSC transition into bipolar stage from multipolar stage[44]. The disparity can be partially explained by the fact that *in vivo*, CS is presented along with adhesion proteins such as laminin and fibronectin within the ECM of the brain, while *in vitro*, CS is introduced to NSCs in a much higher concentration or without any adhesion site. In this study, we conjugated synthetic adhesion peptide to address this problem to focus on the effect of CS sulfonation on NSC behavior in brain-like environment. NSCs actively secrets pleiotrophin, which mediates neuronal migration upon binding[45], and over sulfated CS binds pleiotrophin with high affinity[46]. Furthermore, over sulfated CS has shown to bind midkine, also identified to induce migration[47]. Together, we suspect that CS-E rich hydrogel enhanced cell motility via growth factor retention, a similar mechanism that promoted proliferation.

Cell-cell contact among hNSCs is critical for survival and self-renewal[48]. Maintaining the direct cell-cell contact upregulates the expression of neurotrophic factors and activation of MAPK signaling, which leads to enhanced hNSC survival, proliferation, as well as neuronal differentiation[49]. Moreover, studies show that the population doubling time of the hNSCs correlates negatively to neutrosphere size and reaches plateau around 250 μm in diameter[50]. Thus, increased hNSC aggregation in CS-E rich hydrogel encouraged cell- cell contact and likely contributed to observed enhanced proliferation. The underlying mechanism for CS-E promoted cell-cell contact needs further experimentation to identify. One possible mechanism is CS-E entrapping signaling molecules secreted by hNSCs and creating strong attraction force, rather than diffused gradient guidance[51]. Therefore, promoting cell-cell communication and recognition among hNSCs within the vicinity. Here, what we refer as “high migration potential” is still relatively slow and only applies to *in vitro* setting. Also, z-axis movement was not accounted for

live-cell imaging, and only took place in x and y-dimensions. Additional studies with 3-dimensional imaging can point to other factors governing increased aggregation.

3.2.5 CS-A rich hydrogel supports neuritogenesis and neuronal activity. Finally, we tested if the degree of sulfation in CS hydrogels affects neuronal functionality upon hNSC differentiation (Figure 6). Differentiated hNSCs were seeded on crosslinked CS hydrogels and were allowed to form networks over a period of 48 hours. The average firing rate of differentiated hNSCs was calculated based on calcium spikes of active neurons detected using Fluo4-AM imaging. Both CS-A and CS-E rich hydrogels supported neural activity with no significant difference (Mann-Whiteney Rank Sum, $p=0.633$). Following calcium imaging, differentiated hNSCs were further stained with B3T and DAPI to characterize the neural network formed (Figure 7). Positive correlation was observed between neurite length and neurite area occupied by differentiated hNSCs in CS-A rich hydrogel ($r=0.42$, $p=0.01$, Pearson's correlation), while low correlation was observed in CS-E rich hydrogels ($r=0.24$, $p=0.20$, Pearson's corrleation; Figure 7C). In addition, circularity of differentiated hNSC clusters in CS hydrogels were examined (Figure 7D). Similar to the correlation data, neurites in CS-E rich hydrogels did not extend their processes away from their cell body and most of the neurites resided close to their origin cell, maintaining closer to spherical shapes (median=0.147). Neuritogenesis in CS-A rich hydrogel was enhanced as circularity value of cell clusters was closer to 0 (median=0.116; Mann-Whitney Rank Sum test, $p<0.05$), meaning neurites were extruding and making connections.

Since perineuronal net ECM is abundant in CS-A (~80-90%)[52], CS-A rich hydrogel was expected to provide more stable support for differentiated hNSCs and promote more robust firing activities. CS-A to CS-E ratio gradually increases as the brain matures and the formation of perineuronal nets by CSPGs terminates the critical period, constructing a secure microenvironment

with little room for plastic changes[53]. Change in CS-A to CS-E ratio in the adult brain has a negative impact in neural connectivity as demonstrated in injured brain, upregulation of CS-E in glial scar contributes to neurite inhibitory microenvironment that hinders network reformation[54]. The potent neurite inhibitory effect of CS-E was confirmed by studying the neural cell morphology in CS-E rich hydrogels. However, neural cells within each island/cluster were able to stay active despite the lack of extensive dendritic/axonal connections, which in the long-term, will fail to form mature network relaying highly synchronized bursts. On the other hand, CS-A rich hydrogel has the potential to serve as a great medium for a matured network to function efficiently, since it allowed neural cell clusters to form robust connections. Due to imaging limitation, differentiated hNSCs were simply overlaid on top of the hydrogel, rather than being encapsulated to form a true 3D network. Future studies should use more sensitive measures, such as viral transduction of neurons with calcium sensors combined with multi-photon scanning microscopy[55], to overcome this issue.

3.3 Conclusion

In summary, we demonstrate here a highly customizable CS hydrogel, prepared utilizing strain-promoted "click" chemistry. These CS hydrogels can be easily tailored to obtain variable physical, rheological, and biochemical properties such as varying CS content, changing pore size and storage modulus, and introducing functional peptides. By altering the sulfation degree of CSs, we showed that CS hydrogels with higher CS-E to CS-A ratio enhanced the migration of hNSCs, which consequently led to enhanced cell-cell contact via the formation of larger hNSC aggregates. We speculate this is a contributing factor for increased proliferation of hNSCs encapsulated in CS-E rich hydrogels. Furthermore, we demonstrated the use of CS-A rich hydrogel as a stable 3D construct to support neural connectivity and activity.

As the adult brain has limited regenerative capacity and cannot repair large scale injuries, stem cell transplantation has been explored to restore the lost tissue and functions[56]. Providing suitable microenvironment for transplanted cells is critical to achieve full integration of these cells functionally, since the long-term survival of transplanted cells has become the major hurdle in the field of stem cell therapy[57]. Understanding the naïve brain ECM and applying it to engineered brain tissue construct will promote graft-host interaction leading to long-term integration. We believe our CS hydrogel can be ultimately used in tissue replacement therapies, in which the CS hydrogel is tailored to match the distinct naïve ECM microenvironment in brain regions, such as prefrontal cortex, and hippocampus, to support area-specific function.

3.4 EXPERIMENTAL METHODS

3.4.1. Chemical synthesis. *Preparation of azide-PEG-amine linker* [21]. For the synthesis of triflyl azide (TfN_3), a premixed solution of CH_2Cl_2 (5 mL) and sodium azide (1.14 g, 17.67 mmol) in water (4 mL) was cooled down to 0 °C. Next, Tf_2O (0.6 mL, 3.53 mmol) in CH_2Cl_2 (5 mL) was added dropwise to the above stirring solution over a period of 1h. After 4h, the layers were separated, and aqueous layer was extracted with CH_2Cl_2 (2 x 10 mL). The combined organic layer was further washed with satd. Na_2CO_3 (20 mL) and used for subsequent step without further purification. 2,2′-(Ethylenedioxy)bis(ethylamine) (1, 1.03 g, 7.06 mmol) in MeOH (10 mL) was added to stirring solution of K_2CO_3 (0.58 g, 4.2 mmol) and $CuSO_4.5H_2O$ (cat. 5 mg) in water (4 mL). The TfN_3 extract was added dropwise over a period of 5h, and the reaction mixture was stirred for another 36h. Organic layer was separated, dried (Na_2SO_4) and concentrated to

afford an oil which was further purified by flash chromatography using CH_2Cl_2/MeOH, 9/1 as eluent to afford desired compound 2 as a colorless oil.

Preparation of DIBO-PEG-amine linker (3). To the stirring solution of 1 (0.190 mL, 1.29 mmol) and *p*-nitrophenol-dibenzocyclooctane (50 mg, 0.129 mmol) in CH_2Cl_2 (20 mL), Et_3N (90.5 μL, 0.64 mmol) was added dropwise. The reaction mixture was stirred for 3 h, after which the solvent was removed under reduced pressure. The residue obtained was purified by flash chromatography using MeOH/CH_2Cl_2, 8 to 30%, v/v to give 3 as a light-yellow oil (41 mg, 80%)

Preparation of CS-E (5). Chemical *O*-sulfation of CS-A (4, from bovine trachea, Sigma Aldrich, MO) was achieved following reported procedures[58]. Briefly, 0.5g of 4 was dissolved in formamide (6.7mL, Sigma Aldrich, MO), and of triethylamine sulfur trioxide complex (0.75 g, Sigma Aldrich, MO) was added to the solution. The reaction was heated to 60°C and allowed to proceed overnight with vigorous stirring under an argon blanket. Next day, the mixture was transferred to aqueous ethanol (7.5mL, 95% v/v), and the mixture was held at room temperature for 30 minutes. 1% aqueous NaCl (~37.3mL) was added, and the pH was adjusted to 7 using 2M NaOH. After dialysis, the solution was lyophilized to yield crude sulfated product. The crude product was dissolved in aqueous NaCl (7.5mL, 16% v/v) and added ethanol to allow precipitation. After centrifugation at 4000 rpm, the pellet was re-suspended in deionized water and the solution was dialyzed. The dialysate was lyophilized, aliquoted and stored in desiccant at −20°C.

Preparation of azide-functionalized CS-A (6) and CS-E (7). 0.5g of CS-A was dissolved in a mixture of water/dimethyl sulfoxide (30 mL, 2/1, v/v). Next, 1-Ethyl-3-(3-dimethylaminopropyl) carbodiimide (438 g, 2.27 mmol, EDC, Thermo, MA) and N-hydroxysuccinimide (131 g, 1.13 mmol, NHS, Thermo, MA) were added and left stirring for an hour. A solution of 2 (molar ratio

to CS=0.6, 0.63 mmol) in DMSO (10 mL) was added dropwise and the resulting reaction mixture was left stirring at room temperature. After 24 hours, the reaction mixture was dialyzed for 3 days against water using 1000 MWCO dialysis tubing (Spectrum Laboratories Inc., CA). Dialyzed Azido-CS-A thus obtained was filtered using a 0.2 µm filter (Thermo, MA) and lyophilized to afford the desired compound 6 as a white fluffy solid. Azido-CS-E (7) was synthesized using the same methods from 5.

Preparation of DIBO-functionalized CS-A (8). To the stirring solution of 4 (0.5 g) in mixture of water/DMSO (1/2, 30 mL), EDC (438 g, 2.27 mmol) and NHS (131 g, 1.13 mmol) were added and stirred for 1h at room temperature. To the above solution, 3 (molar ratio to CS=0.6, 0.63 mmol) in DMSO (10 mL) was added dropwise and left stirring for another 24h. Next, the reaction mixture was dialyzed for 3 days against water using 1000 MWCO dialysis tubing (Spectrum Laboratories Inc., CA), filtered (0.2 µm) and lyophilized to afford the desired compound 8 as a white fluffy solid.

Synthesis of fusion peptide. Peptide was synthesized on a rink amide resin (Novabiochem, San Diego, CA, 0.1 mmol) by established protocols on a CEM Liberty Automated Microwave Peptide Synthesizer using standard Fmoc-protected amino acids. Azide group was introduced by using Fmoc-Lys(N3)-OH as the terminal amino acid. FP was purified by high-pressure liquid chromatography (HPLC) and characterized using MS (MALDI-ToF, Applied Biosystems 5800).

3.4.2. Hydrogel preparation. Lyophilized DIBO-CS-A (8) and Azido-CS-A (6) or CS-E (7) were each dissolved in neurobasal medium (Thermo, MA) to achieve wt/v concentration of 3% and 10%. These stock solutions were diluted with expansion medium (1x neurobasal medium, 2% B-27 (Thermo, MA), 100x NEAA (Corning, NY), 2mM Glutamax (Corning, NY), 20ng/ml FGF2 (R&D Systems, MN)), and then mixed gently by pippeting to initiate gelation at room

temperature to yield desired final concentrations. Stable hydrogel was formed within 10 minutes of incubation as confirmed by vial-tilting method.

3.4.3. Scanning Electron Microscopy (SEM). The microarchitecture of hydrogels was observed using a Zeiss 1450EP scanning electron microscope (Zeiss, NY). Briefly, hydrogels were casted in polydimethylsiloxane (PDMS) molds, frozen at -80°C, and then lyophilized for 24 hours. Lyophilized gels were mounted on 10 mm stubs and coated with gold for 60 seconds in a Module Sputter Coater (SPI, PA) before being imaged at accelerating voltage of 20 kV. Average pore size of hydrogels was calculated using ImageJ.

3.4.4. Rheology. Hydrogel mixtures were dispensed in 16 mm diameter circular PDMS molds to form 1 mm thick discs. Each of the resulting hydrogels were overlaid with 500 uL of PBS and incubated at 37 °C overnight. Rheological testing was performed using a parallel plate rheometer (Anton Paar, CA). Frequency sweep experiments from 0.1-100 Hz at 5% strain were performed at 37 °C in triplicate.

3.4.5. Swelling and Degradation studies. 250 uL of 2.5% DIBO/1% Azido-CS-A hydrogel was casted in a pre-weighed glass bottom dish and the initial weight was obtained. Then, it was overlaid with 250 uL of PBS and incubated at 37°C/ 5% CO_2 with 95% humidity. The next day, media was removed and the glass bottom dish with hydrogel was weighed to determine the degree of swelling. This process was repeated for 14 days. For the degradation assay, the same procedure was conducted with PBS containing 33 mU of hyaluronidase (MP Biomedicals, CA).

3.4.6. Hydrogel encapsulation of hNSCs. Human neural stem cells (hNSCs) were suspended in 3% DIBO-CS-A, and 10% Azido-CS-A to yield 2.5% DIBO/1% Azido-CS gel at a concentration of 5×10^6 cells/mL. The mixture was quickly dispensed onto a glass bottom dish. Hydrogels were overlaid with expansion media upon gelation and incubated at 37°C/ 5% CO_2.

3.4.7. Immunohistochemistry. hNSCs encapsulated in hydrogels were fixed in 4% paraformaldehyde (PFA) with 0.4 M sucrose in PBS, rinsed thrice in PBS, and incubated in blocking buffer (4% goat serum, 0.5% Triton-X100 in PBS). After an hour, fresh blocking buffer containing primary antibodies was added to stain for: sox1 (R&D Systems, MN), nestin (Millipore, CA), focal adhesion kinase (Novax, CA), vinculin (Sigma, MO), and class III β-tubulin (Millipore, CA). After overnight incubation at 4 °C, hydrogels were then rinsed thrice in PBS and incubated in blocking buffer for 3 hours with secondary antibodies (Alexa Fluor 488, 555 and 647; Thermo, MA). Following three washes of PBS, hydrogels were incubated with a nuclear stain (DAPI; Thermo, MA) in PBS for 10 min, rinsed thrice in PBS and mounted with fluoromount-G (SouthernBiotech, AL). Cells were imaged using Zeiss LSM 710 confocal microscope (Zeiss, Germany).

3.4.8. Proliferation assay. hNSCs were encapsulated and cultured in either CS-A or CS-E hydrogel over 2 days. EdU proliferation kit (Abcam, MA) was used to assess hNSC proliferation. Briefly, 10mM EdU stock was diluted in expansion media at 1:1000 followed by 3 hours of cell incubation. Subsequently, cells were rinsed and accutase (Sigma-Aldrich, MO) was added to separate cells from the gel. Isolated cells were fixed with 4% PFA. After permeabilizing the cells with the provided buffer, cells were incubated in the reaction mixture containing iFluor 488 azide for 30 minutes. Cells were rinsed twice and diluted in Hoechst (1ug/mL; Thermo, MA) containing PBS for flow cytometry (NovoCyte Quanteon, Agilent Technologies Inc., USA) at Ex/Em = 491/520 nm. Raw data was processed using FlowJo software (Version 10.2. Ashland). Representative images were taken with Zeiss LSM 710 confocal microscope (Biomedical Microscopy Core, UGA). Cells for representative images were not separated from the gel but kept in hydrogel and proceeded to the following steps.

3.4.9. Cell Migration assay. hNSCs were stained with Hoechst (1 ug/mL; Thermo, MA) and DiO (5ug/mL; Thermo, MA) for 20 minutes in serum free neurobasal media for 20 minutes and rinsed twice in expansion media before encapsulation. hNSCs were encapsulated following the above protocol on a 35 mm single glass-bottom dish. Immediately upon gelation (10 minutes), hNSCs were overlaid with expansion media and imaged over 1 hour using an Inverted Fluor Polarizing Microscope (Leica DM IRBE; Leica Microsystems, Buffalo Grove, IL). Images were obtained every 10 minutes. Cells were maintained in Tokai live cell culture stage adapter at 37°C with a flow of 5% CO_2 medical grade air mixture (Airgas, PA) during the recording session. Migration speed was calculated using Volocity software (PerkinElmer, MA).

3.4.10. Neural activity imaging. hNSCs were allowed to differentiate for 7 days prior to encapsulation. Differentiated hNSCs were collected and overlaid on top of crosslinked CS hydrogels on 35 mm single glass-bottom dish. After 48 hours, a stock solution was made using 50 ug of Fuo4-AM (Thermo, MA) dissolved in 20% F127 pluronic acid in DMSO (v/v). A loading solution was made by adding 4 uL of stock Fluo4-AM solution to expansion media. Media was replaced with pre-warmed loading solution and the cells were incubated for 20 minutes. Cells were then transferred to Brainphys® only solution for recording. Calcium recording was performed using Leica IRDBE inverted microscope with a TRITC filter (Ex/Em: 561/576 nm). Images were obtained for 5 mins at 1 frame per sec with 0.5 sec exposure. Cells were maintained in Tokai live cell culture stage adapter at 37°C with a flow of 5% CO_2 medical grade air mixture (Airgas, PA) during the recording session. Recorded time lapses were processed using MATLAB®. Cell soma were detected using maximum intensity projection and regions of interest were automatically defined using custom-made scripts in MATLAB® with

the image analysis toolbox. Calcium activity traces were extracted from ROI and the spikes were detected using normalized DF/F and peak detection using MATLAB®.

3.4.11. Image Analysis and Statistics. Fiji[59] was used to process the raw images obtained for co-localization (Coloc2 plugin) of vinculin/FAK and sox1/DAPI. Neurite length was calculated using published automated quantification method, NeuriteTracer[60]. Aggregation size based on Nestin+ area and circularity based on B3T were calculated using built-in functions in Fiji[59]. Sigmaplot was used to evaluate the significance ($p<0.05$) between groups either using the student t-test (normal data distribution) or the Mann-Whitney Rank Sum test (when failed normal distribution). Graphs were created using RStudio (Boston, MA). All experiments were performed in triplicate.

3.5 References

1 Hemphill, M. A., Dauth, S., Yu, C. J., Dabiri, B. E. & Parker, K. K. Traumatic Brain Injury and the Neuronal Microenvironment: A Potential Role for Neuropathological Mechanotransduction. *Neuron* **85**, 1177-1192, doi:10.1016/j.neuron.2015.02.041 (2015).

2 Ruoslahti, E. Brain extracellular matrix. *Glycobiology* **6**, 489-492, doi:10.1093/glycob/6.5.489 (1996).

3 Cembran, A., Bruggeman, K. F., Williams, R. J., Parish, C. L. & Nisbet, D. R. Biomimetic Materials and Their Utility in Modeling the 3-Dimensional Neural Environment. *iScience* **23**, 100788, doi:10.1016/j.isci.2019.100788 (2020).

4 Schwartz, N. B. & Domowicz, M. S. Proteoglycans in brain development and pathogenesis. *FEBS Lett* **592**, 3791-3805, doi:10.1002/1873-3468.13026 (2018).

5 Avram, S., Shaposhnikov, S., Buiu, C. & Mernea, M. Chondroitin sulfate proteoglycans: structure-function relationship with implication in neural development and brain disorders. *Biomed Res Int* **2014**, 642798, doi:10.1155/2014/642798 (2014).

6 Nicholson, C. & Sykova, E. Extracellular space structure revealed by diffusion analysis. *Trends Neurosci* **21**, 207-215, doi:10.1016/s0166-2236(98)01261-2 (1998).

7 Silbert, J. E. & Sugumaran, G. Biosynthesis of chondroitin/dermatan sulfate. *IUBMB Life* **54**, 177-186, doi:10.1080/15216540214923 (2002).

8 Lindahl, U. & Hook, M. Glycosaminoglycans and their binding to biological macromolecules. *Annu Rev Biochem* **47**, 385-417, doi:10.1146/annurev.bi.47.070178.002125 (1978).

9 Zhang, Z., Ohtake-Niimi, S., Kadomatsu, K. & Uchimura, K. Reduced molecular size and altered disaccharide composition of cerebral chondroitin sulfate upon Alzheimer's pathogenesis in mice. *Nagoya J Med Sci* **78**, 293-301 (2016).

10 Liu, Z. *et al.* Glycosaminoglycans of the porcine central nervous system. *Biochemistry* **49**, 9839-9847, doi:10.1021/bi101305b (2010).

11 Djerbal, L., Lortat-Jacob, H. & Kwok, J. Chondroitin sulfates and their binding molecules in the central nervous system. *Glycoconj J* **34**, 363-376, doi:10.1007/s10719-017-9761-z (2017).

12 Mizumoto, S., Fongmoon, D. & Sugahara, K. Interaction of chondroitin sulfate and dermatan sulfate from various biological sources with heparin-binding growth factors and cytokines. *Glycoconj J* **30**, 619-632, doi:10.1007/s10719-012-9463-5 (2013).

13 Deepa, S. S., Umehara, Y., Higashiyama, S., Itoh, N. & Sugahara, K. Specific molecular interactions of oversulfated chondroitin sulfate E with various heparin-binding growth factors. Implications as a physiological binding partner in the brain and other tissues. *J Biol Chem* **277**, 43707-43716, doi:10.1074/jbc.M207105200 (2002).

14 Gama, C. I. *et al.* Sulfation patterns of glycosaminoglycans encode molecular recognition and activity. *Nat Chem Biol* **2**, 467-473, doi:10.1038/nchembio810 (2006).

15 Shipp, E. L. & Hsieh-Wilson, L. C. Profiling the sulfation specificities of glycosaminoglycan interactions with growth factors and chemotactic proteins using microarrays. *Chem Biol* **14**, 195-208, doi:10.1016/j.chembiol.2006.12.009 (2007).

16 Sirko, S. *et al.* Chondroitin sulfates are required for fibroblast growth factor-2-dependent proliferation and maintenance in neural stem cells and for epidermal growth factor-dependent migration of their progeny. *Stem Cells* **28**, 775-787, doi:10.1002/stem.309 (2010).

17 Dickendesher, T. L. *et al.* NgR1 and NgR3 are receptors for chondroitin sulfate proteoglycans. *Nat Neurosci* **15**, 703-712, doi:10.1038/nn.3070 (2012).

18 Dyck, S. *et al.* Perturbing chondroitin sulfate proteoglycan signaling through LAR and PTPsigma receptors promotes a beneficial inflammatory response following spinal cord injury. *J Neuroinflammation* **15**, 90, doi:10.1186/s12974-018-1128-2 (2018).

19 Hein, C. D., Liu, X. M. & Wang, D. Click chemistry, a powerful tool for pharmaceutical sciences. *Pharm Res* **25**, 2216-2230, doi:10.1007/s11095-008-9616-1 (2008).

20 Hou, J., Liu, X., Shen, J., Zhao, G. & Wang, P. G. The impact of click chemistry in medicinal chemistry. *Expert Opin Drug Discov* **7**, 489-501, doi:10.1517/17460441.2012.682725 (2012).

21 Zhao, Z., Loane, D. J., Murray, M. G., 2nd, Stoica, B. A. & Faden, A. I. Comparing the predictive value of multiple cognitive, affective, and motor tasks after rodent traumatic brain injury. *J Neurotrauma* **29**, 2475-2489, doi:10.1089/neu.2012.2511 (2012).

22 Jin, J. *et al.* Effect of chondroitin sulfate proteoglycans on neuronal cell adhesion, spreading and neurite growth in culture. *Neural Regen Res* **13**, 289-297, doi:10.4103/1673-5374.226398 (2018).

23 Lau, L. W., Cua, R., Keough, M. B., Haylock-Jacobs, S. & Yong, V. W. Pathophysiology of the brain extracellular matrix: a new target for remyelination. *Nat Rev Neurosci* **14**, 722-729, doi:10.1038/nrn3550 (2013).

24 Ernst, H., Zanin, M. K., Everman, D. & Hoffman, S. Receptor-mediated adhesive and anti-adhesive functions of chondroitin sulfate proteoglycan preparations from embryonic chicken brain. *J Cell Sci* **108 (Pt 12)**, 3807-3816 (1995).

25 Sahab Negah, S., Khooei, A., Samini, F. & Gorji, A. Laminin-derived Ile-Lys-Val-ala-Val: a promising bioactive peptide in neural tissue engineering in traumatic brain injury. *Cell Tissue Res* **371**, 223-236, doi:10.1007/s00441-017-2717-6 (2018).

26 Karumbaiah, L. *et al.* Chondroitin Sulfate Glycosaminoglycan Hydrogels Create Endogenous Niches for Neural Stem Cells. *Bioconjug Chem* **26**, 2336-2349, doi:10.1021/acs.bioconjchem.5b00397 (2015).

27 Fallenstein, G. T., Hulce, V. D. & Melvin, J. W. Dynamic mechanical properties of human brain tissue. *J Biomech* **2**, 217-226, doi:10.1016/0021-9290(69)90079-7 (1969).

28 Axpe, E., Orive, G., Franze, K. & Appel, E. A. Towards brain-tissue-like biomaterials. *Nat Commun* **11**, 3423, doi:10.1038/s41467-020-17245-x (2020).

29 Modo, M. Bioscaffold-Induced Brain Tissue Regeneration. *Front Neurosci* **13**, 1156, doi:10.3389/fnins.2019.01156 (2019).

30 Logun, M. T. *et al.* Glioma Cell Invasion is Significantly Enhanced in Composite Hydrogel Matrices Composed of Chondroitin 4- and 4,6-Sulfated Glycosaminoglycans. *J Mater Chem B* **4**, 6052-6064, doi:10.1039/C6TB01083K (2016).

31 Venere, M. *et al.* Sox1 marks an activated neural stem/progenitor cell in the hippocampus. *Development* **139**, 3938-3949, doi:10.1242/dev.081133 (2012).

32 Gage, F. H. Mammalian neural stem cells. *Science* **287**, 1433-1438, doi:10.1126/science.287.5457.1433 (2000).

33 Ponti, G. *et al.* Cell cycle and lineage progression of neural progenitors in the ventricular-subventricular zones of adult mice. *Proc Natl Acad Sci U S A* **110**, E1045-1054, doi:10.1073/pnas.1219563110 (2013).

34 Zheng, W., Nowakowski, R. S. & Vaccarino, F. M. Fibroblast growth factor 2 is required for maintaining the neural stem cell pool in the mouse brain subventricular zone. *Dev Neurosci* **26**, 181-196, doi:10.1159/000082136 (2004).

35 Kang, W. & Hebert, J. M. FGF Signaling Is Necessary for Neurogenesis in Young Mice and Sufficient to Reverse Its Decline in Old Mice. *J Neurosci* **35**, 10217-10223, doi:10.1523/JNEUROSCI.1469-15.2015 (2015).

36 Kelly, C. M., Zietlow, R., Dunnett, S. B. & Rosser, A. E. The effects of various concentrations of FGF-2 on the proliferation and neuronal yield of murine embryonic neural precursor cells in vitro. *Cell Transplant* **12**, 215-223, doi:10.3727/000000003108746777 (2003).

37 Nikitovic, D. *et al.* Chondroitin sulfate and heparan sulfate-containing proteoglycans are both partners and targets of basic fibroblast growth factor-mediated proliferation in human metastatic melanoma cell lines. *Int J Biochem Cell Biol* **40**, 72-83, doi:10.1016/j.biocel.2007.06.019 (2008).

38 Ramachandra, R. *et al.* Brittlestars contain highly sulfated chondroitin sulfates/dermatan sulfates that promote fibroblast growth factor 2-induced cell signaling. *Glycobiology* **24**, 195-207, doi:10.1093/glycob/cwt100 (2014).

39 Kanemura, Y. *et al.* In vitro screening of exogenous factors for human neural stem/progenitor cell proliferation using measurement of total ATP content in viable cells. *Cell Transplant* **14**, 673-682 (2005).

40 Wozniak, M. A., Modzelewska, K., Kwong, L. & Keely, P. J. Focal adhesion regulation of cell behavior. *Biochim Biophys Acta* **1692**, 103-119, doi:10.1016/j.bbamcr.2004.04.007 (2004).

41 Kumar, A., Placone, J. K. & Engler, A. J. Understanding the extracellular forces that determine cell fate and maintenance. *Development* **144**, 4261-4270, doi:10.1242/dev.158469 (2017).

42 Vining, K. H. & Mooney, D. J. Mechanical forces direct stem cell behaviour in development and regeneration. *Nat Rev Mol Cell Biol* **18**, 728-742, doi:10.1038/nrm.2017.108 (2017).

43 Galindo, L. T. *et al.* Chondroitin Sulfate Impairs Neural Stem Cell Migration Through ROCK Activation. *Mol Neurobiol* **55**, 3185-3195, doi:10.1007/s12035-017-0565-8 (2018).

44 Ishii, M. & Maeda, N. Oversulfated chondroitin sulfate plays critical roles in the neuronal migration in the cerebral cortex. *J Biol Chem* **283**, 32610-32620, doi:10.1074/jbc.M806331200 (2008).

45 Tang, C. *et al.* Neural Stem Cells Behave as a Functional Niche for the Maturation of Newborn Neurons through the Secretion of PTN. *Neuron* **101**, 32-44 e36, doi:10.1016/j.neuron.2018.10.051 (2019).

46 Maeda, N., Fukazawa, N. & Hata, T. The binding of chondroitin sulfate to pleiotrophin/heparin-binding growth-associated molecule is regulated by chain length and oversulfated structures. *J Biol Chem* **281**, 4894-4902, doi:10.1074/jbc.M507750200 (2006).

47 Maeda, N. *et al.* A receptor-like protein-tyrosine phosphatase PTPzeta/RPTPbeta binds a heparin-binding growth factor midkine. Involvement of arginine 78 of midkine in the high affinity binding to PTPzeta. *J Biol Chem* **274**, 12474-12479, doi:10.1074/jbc.274.18.12474 (1999).

48 Campos, L. S. Neurospheres: insights into neural stem cell biology. *J Neurosci Res* **78**, 761-769, doi:10.1002/jnr.20333 (2004).

49 Jiao, Q. *et al.* Cell-Cell Connection Enhances Proliferation and Neuronal Differentiation of Rat Embryonic Neural Stem/Progenitor Cells. *Front Cell Neurosci* **11**, 200, doi:10.3389/fncel.2017.00200 (2017).

50 Mori, H. *et al.* Effect of neurosphere size on the growth rate of human neural stem/progenitor cells. *J Neurosci Res* **84**, 1682-1691, doi:10.1002/jnr.21082 (2006).

51 Roy, S. & Kornberg, T. B. Paracrine signaling mediated at cell-cell contacts. *Bioessays* **37**, 25-33, doi:10.1002/bies.201400122 (2015).

52 Deepa, S. S. *et al.* Composition of perineuronal net extracellular matrix in rat brain: a different disaccharide composition for the net-associated proteoglycans. *J Biol Chem* **281**, 17789-17800, doi:10.1074/jbc.M600544200 (2006).

53 Miyata, S. & Kitagawa, H. Mechanisms for modulation of neural plasticity and axon regeneration by chondroitin sulphate. *J Biochem* **157**, 13-22, doi:10.1093/jb/mvu067 (2015).

54 Gilbert, R. J. *et al.* CS-4,6 is differentially upregulated in glial scar and is a potent inhibitor of neurite extension. *Mol Cell Neurosci* **29**, 545-558, doi:10.1016/j.mcn.2005.04.006 (2005).

55 Tehrani, K. F. *et al.* Five-dimensional two-photon volumetric microscopy of in-vivo dynamic activities using liquid lens remote focusing. *Biomed Opt Express* **10**, 3591-3604, doi:10.1364/BOE.10.003591 (2019).

56 Sun, D. The potential of neural transplantation for brain repair and regeneration following traumatic brain injury. *Neural Regen Res* **11**, 18-22, doi:10.4103/1673-5374.169605 (2016).

57 Henriques, D., Moreira, R., Schwamborn, J., Pereira de Almeida, L. & Mendonca, L. S. Successes and Hurdles in Stem Cells Application and Production for Brain Transplantation. *Front Neurosci* **13**, 1194, doi:10.3389/fnins.2019.01194 (2019).

58 Cai, C. *et al.* Semi-synthesis of chondroitin sulfate-E from chondroitin sulfate-A. *Carbohydr Polym* **87**, 822-829, doi:10.1016/j.carbpol.2011.08.075 (2012).

59 Schindelin, J. *et al.* Fiji: an open-source platform for biological-image analysis. *Nat Methods* **9**, 676-682, doi:10.1038/nmeth.2019 (2012).

60 Pool, M., Thiemann, J., Bar-Or, A. & Fournier, A. E. NeuriteTracer: a novel ImageJ plugin for automated quantification of neurite outgrowth. *J Neurosci Methods* **168**, 134-139, doi:10.1016/j.jneumeth.2007.08.029 (2008).

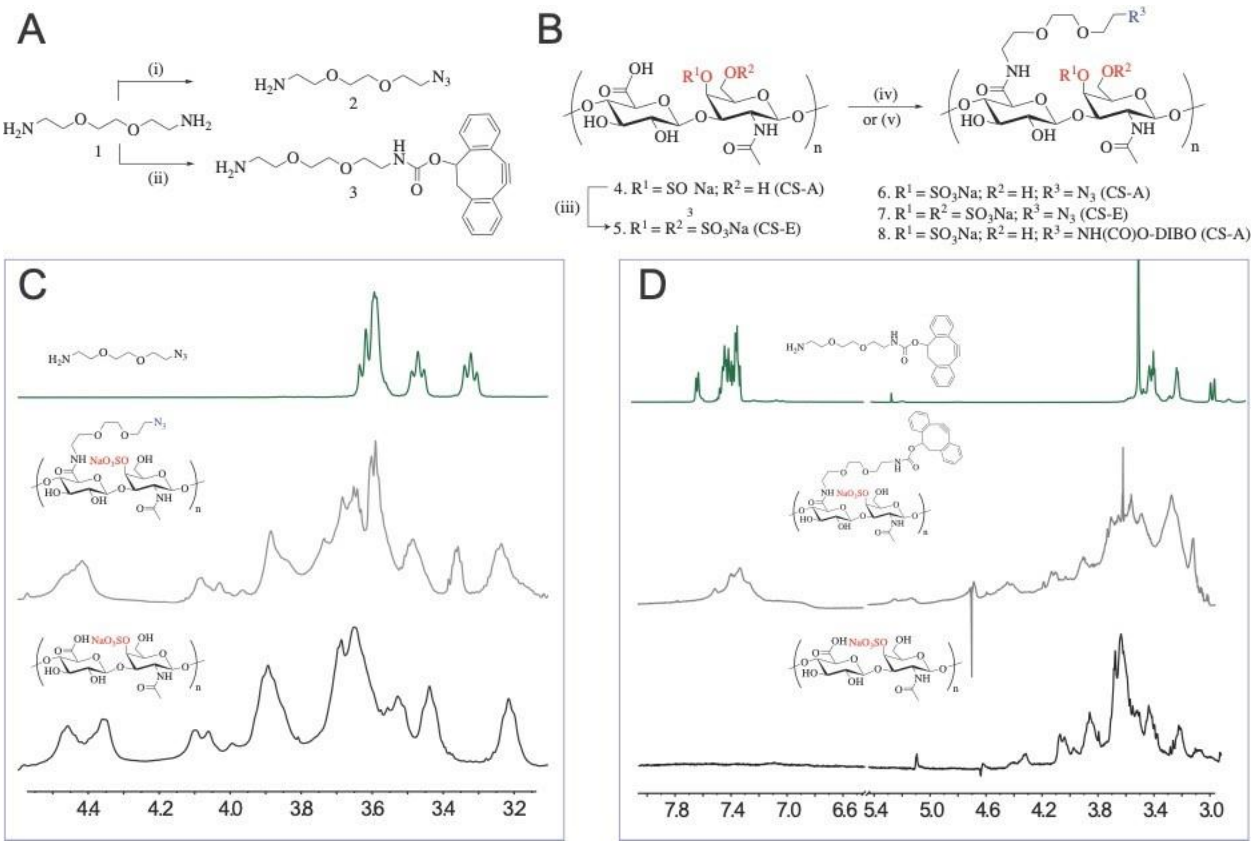

Figure 3.1 (A) Synthesis scheme. Synthesis of PEG-azide and PEG-DIBO linker. (B) Synthesis of azide and DIBO functionalized CS-A and CS-E. *Reagents and conditions*: (i) Tf_2O, NaN_3, K_2CO_3, $CuSO_4.5H_2O$; (ii) EDC, NHS, DMSO/H_2O (4/1), rt, 24 h; (iii) 2, EDC, NHS, DMSO/H_2O (4/1), rt, 24 h (for 6 and 7); (iv) 3, EDC, NHS, DMSO/H_2O (4/1), rt, 24 h (for 8 and 9); (C) H^1 NMR spectra of PEG-azide, CS-azide and CS-GAG from top to bottom. The degree of azide functionalization on CS-A backbone was estimated to be about 35-45%. D) H^1 NMR spectra of PEG-DIBO, CS-DIBO and CS-GAG from top to bottom., showing 10-15% CS-DIBO functionalization.

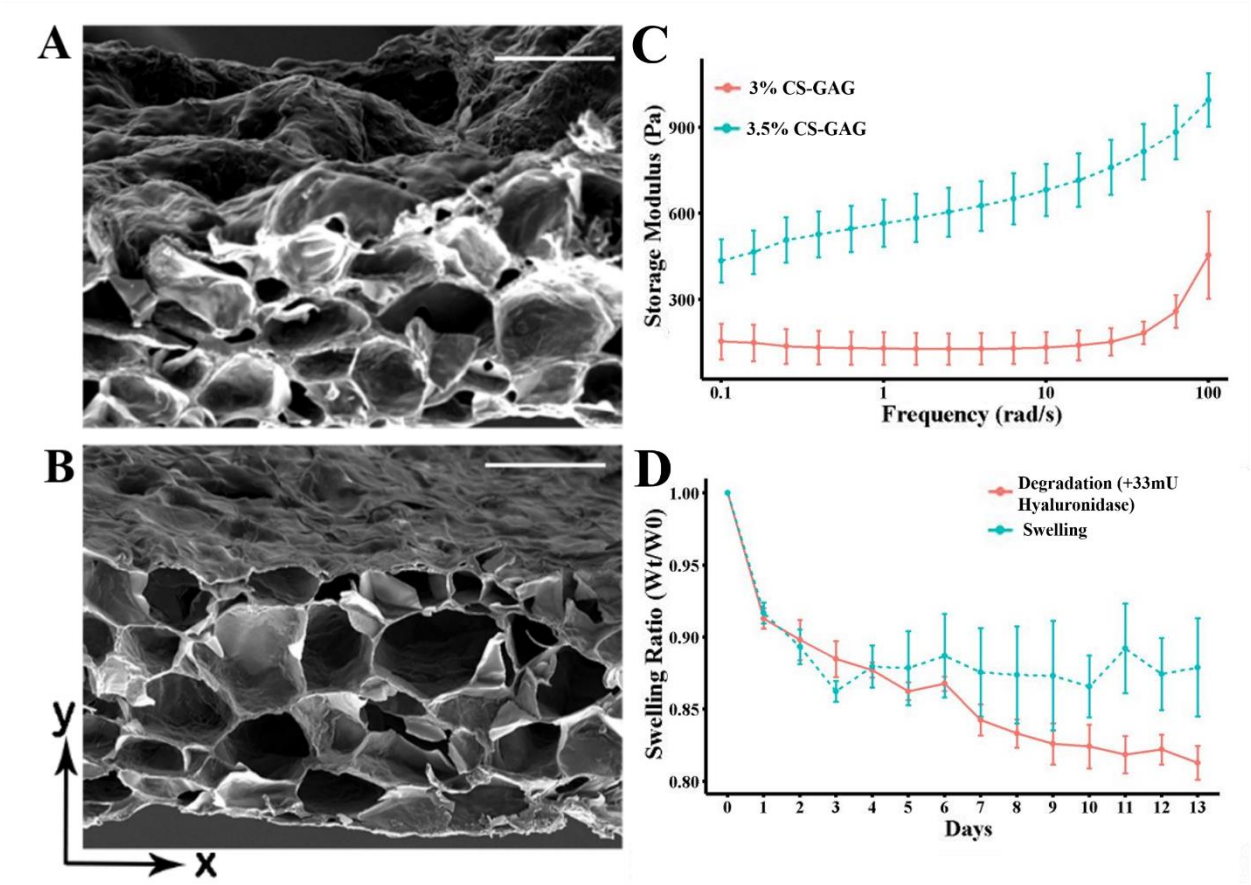

Figure 3.2 Microstructure of hydrogels via SEM imaging revealed the average pore size of A) 3.5% CS hydrogel (17.2±12.0 μm), and B) 3% CS-A hydrogel (25.2±17.5 μm). Scale bar: 100 μm. C) Storage modulus was used to describe the viscoelastic properties of two hydrogels consisting of 3.5 % (2.5% DIBO-CS-A and 1% azido-CS-A), and 3% CS-A (2% DIBO-CS-A and 1% azido-CS-A) content. D) Swelling and degradation of cross-linked hydrogels (3% CS-A) in the presence of 33mU of hyaluronidase over 14 days in vitro.

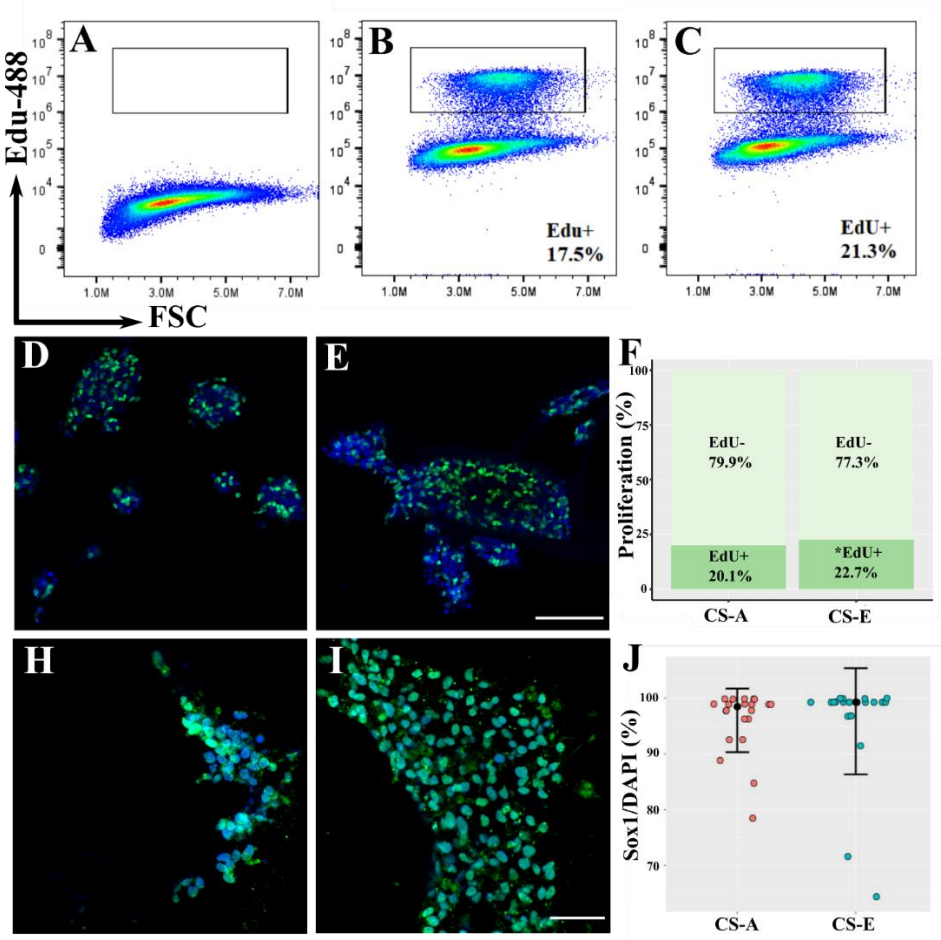

Figure 3.3 NSC proliferation in CS-GAG hydrogels. Proliferating NSCs cultured in CS-GAG hydrogels were determined using flow cytometry. A) Control NSCs not stained with EdU to serve as a negative control. NSCs cultured in B) CS-A and C) CS-E hydrogels. EdU incorporated portion of NSCs has enhanced fluorescence intensity as shown within the square box. Representative images of EdU incorporated NSCs in D) CS-A and E) CS-E hydrogels. Scale bar: 100 µm. F) EdU+ cells/total number of NSCs was compared between NSCs encapsulated in CS-A and CS-E hydrogels. *$p<0.001$ (Chi-square). Representative images of NSCs in H) CS-A and I) CS-E stained with activated stem cell marker, Sox1 (green), and counter stained with DAPI (blue). Scale bar: 40 µm. J) No difference was detected between colocalization values of sox1 over DAPI expressed in NSCs encapsulated in CS-A and CS-E hydrogels.

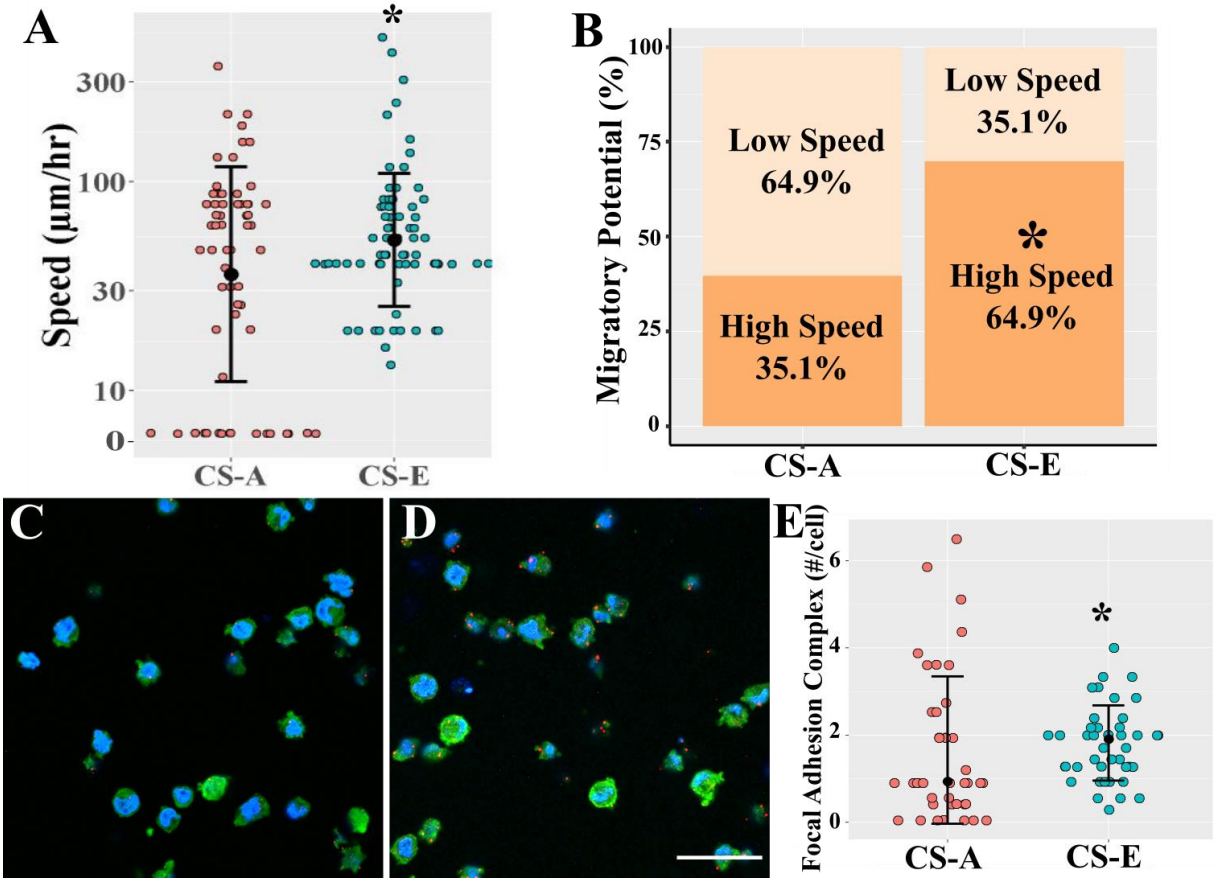

Figure 3.4 Migratory potential. A) NSC migratory speed in CS-A and CS-E hydrogel was measured over 1 hour. Each dot represents an individual cell. B) NSC with migratory speed >30 μm/hr was categorized as cell with high migratory potential. NSCs with high migratory potential over entire NSC population within the ROI was calculated. *p<0.001 (Chi-square). C) Representative images of NSCs in C) CS-A and D) CS-E hydrogels stained with vinculin (green), FAK (red) and DAPI (blue). Scale bar: 30 μm. E) The number of focal adhesion complex/cell was calculated based on the number of FAK puncta colocalized with vinculin. *p=0.034 (Mann-Whitney Rank Sum).

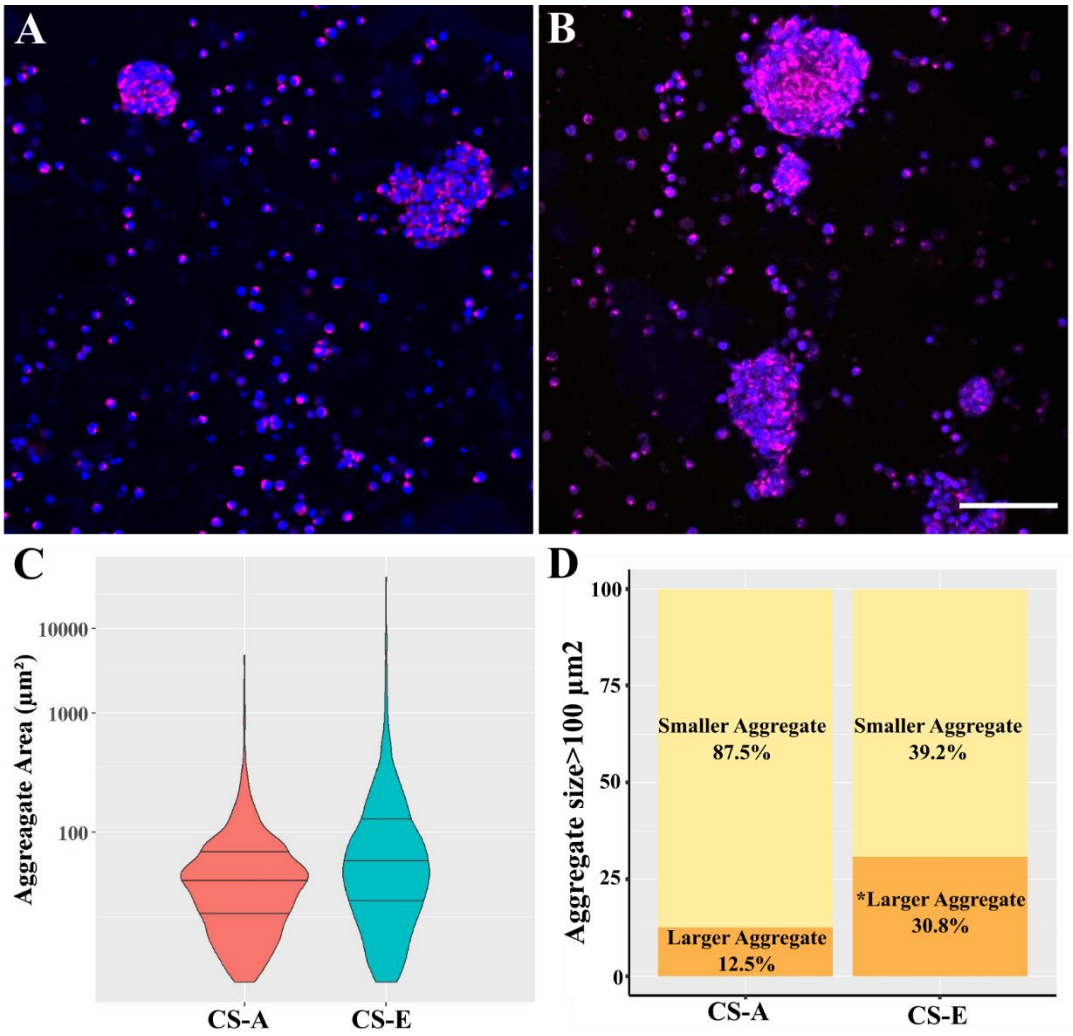

Figure 3.5 NSCs cultured in A) CS-A and B) CS-E hydrogels stained with nestin (magenta), and DAPI (blue). Scale bar: 80 µm. C) NSC aggregate area (2D) was calculated based on the confocal images of nestin overlaid with DAPI. D) Aggregates larger than 100 μm^2 was binned as a population over entire NSC population. a *$p<0.001$ (Chi-square).

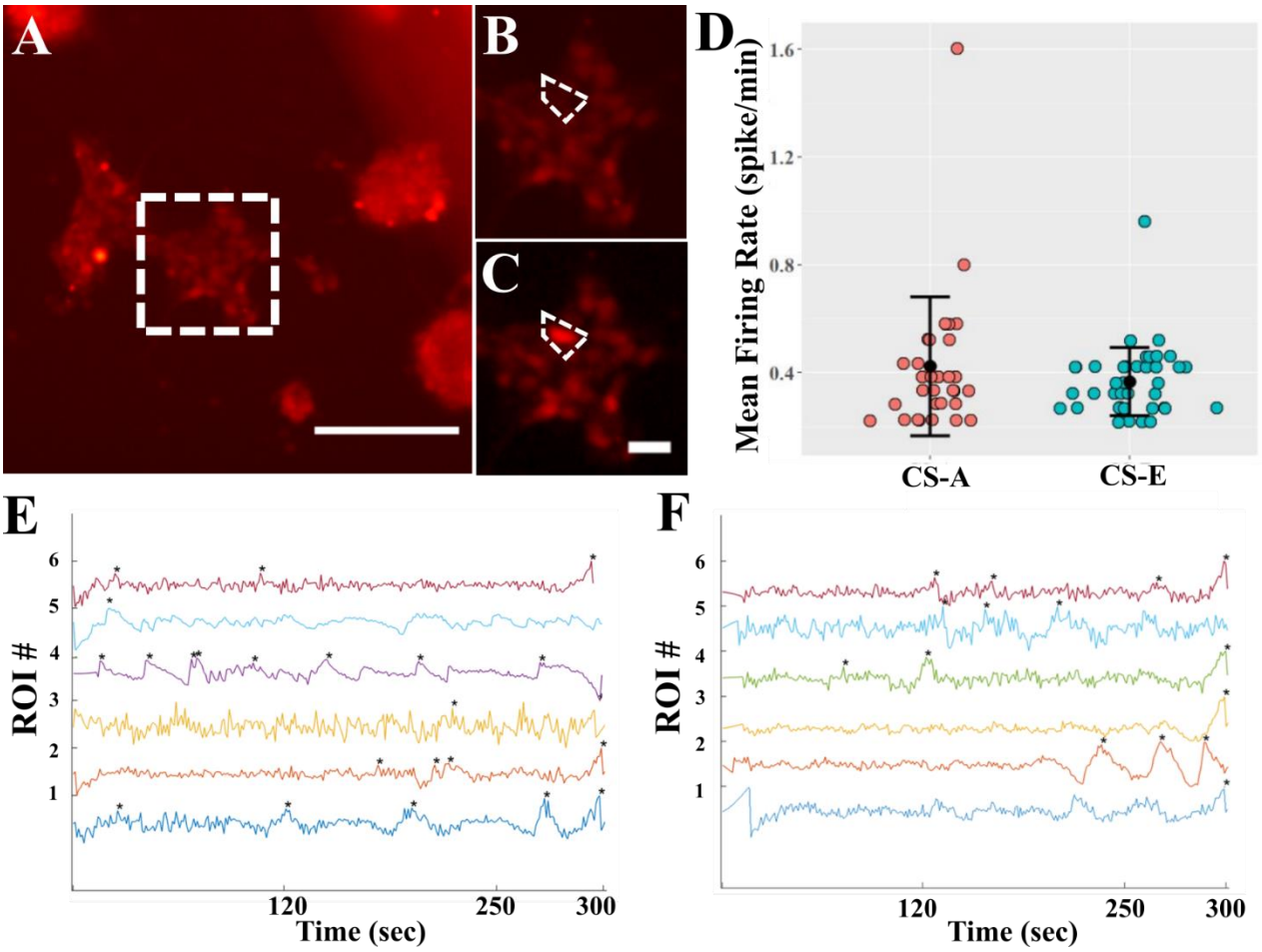

Figure 3.6 A) Snapshot of calcium signal detection in CS-A hydrogel. Scale bar: 25 µm. B,C) White square area was magnified to show change in fluorescence intensity. Scale bar: 5 µm. Dashed area represents an ROI containing a single nucleus. D) Mean firing rate of the active ROIs obtained from Fluo4-AM recordings. Representative extracted calcium traces of Fluo4-AM recording over 5 minutes in E) CS-A and F) CS-E hydrogels. * indicate the detection of a calcium spike from the ΔF/F processed traces.

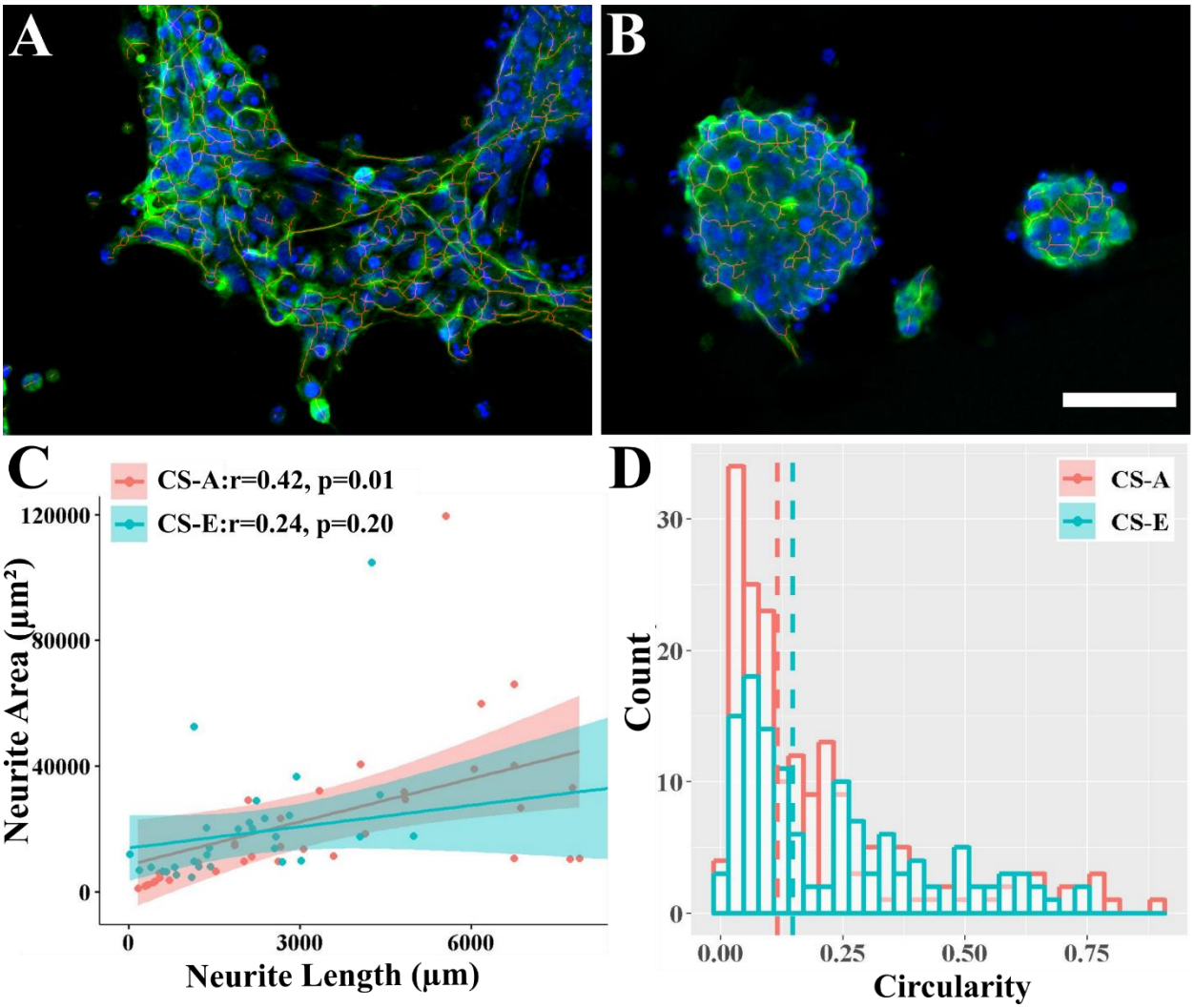

Figure 3.7 Representative images of differentiated hNSCs culture in A) CS-A rich and B) CS-E rich hydrogels, and stained with βIII-tubulin (B3T, green) and DAPI (blue). Red line shows skeletonized neuronal processes. Scale bar: 50 µm. C) Scatter plot showing positive correlation between neurite length and B3T area calculated in CS-E rich hydrogel, while the correlation in CS-A rich hydrogel is low. D) Circularity (1 indicating a perfect circle) of individual aggregate was calculated to determine the degree of neurite extensions. Dashed line marks the mean value for each group.

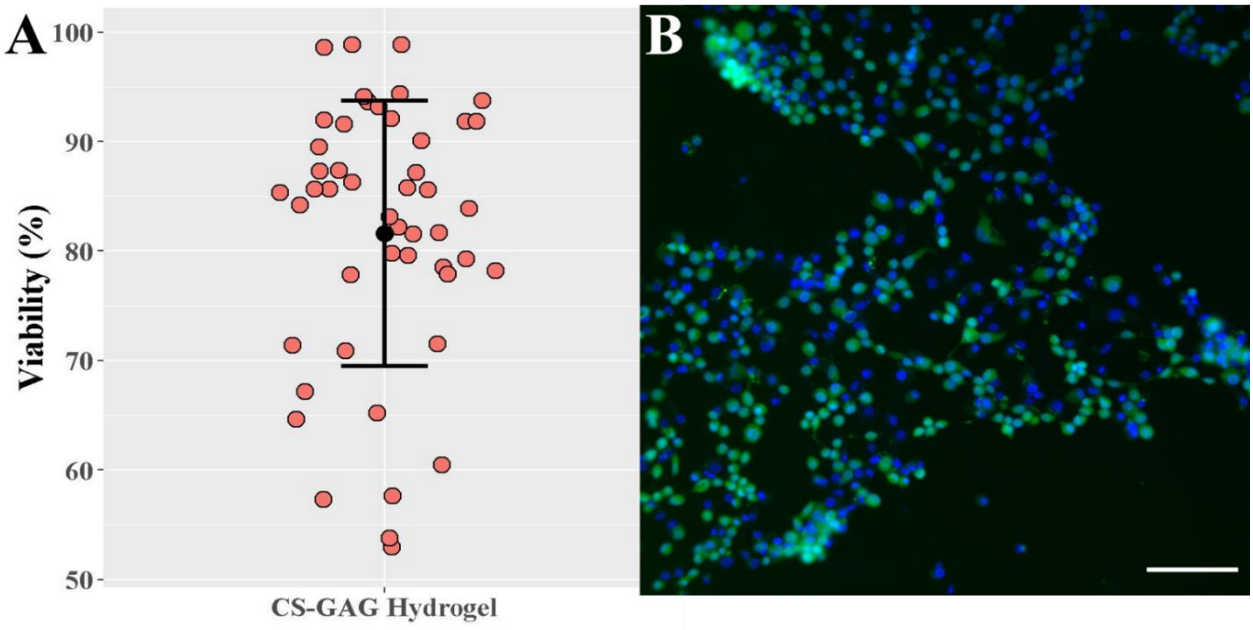

Supplementary Figure 3.1 NSCs viability encapsulated in CS-GAG hydrogel after 48 hours was determined using calcien AM. A) Cell viability determined by % DAPI overlaid with calcien AM (mean± S.D.= 81.6±12.1%). B) Representative image showing healthy NSCs stained with calcien AM (green), and counterstained with DAPI (blue). Scale bar: 200 µm.

CHAPTER 4

DISCUSSION AND CONCLUSION

This dissertation describes two synergistic cell-free approaches that carry therapeutic potential for endogenous tissue and functional repair after sTBI. In these studies, we demonstrated a) the localized neuroprotection, enhanced presence of endogenous NSCs in the lesion site, and attenuated motor function impairments induced by the acute, intravenous delivery of NSC-derived EVs; and b) the effects of sulfation modulation of CS hydrogels on NSC maintenance, migration, and activity of differentiated neurons.

4.1 Effects of NSC-EV Treatment After sTBI

Prior studies have already established the need for acute (within 12 hours) stabilization and treatment of individuals who sustain sTBI in order to mitigate the significant risk of death[1]. However, these procedures require specialist attention at a neuroscience center, which is often not possible within the critical therapeutic time window. There are no effective therapeutics that can be administered during this acute timeframe that can prevent tissue loss and long-term functional deficits. In Chapter 2, we describe preclinical studies that demonstrate the utility of NSC-EVs as a neuroprotective agent that can be acutely administered via the intravenous route after sTBI. The non-cellular attributes of NSC-EVs circumvents pitfalls and risks associated with the unintended inflammatory consequences and uncontrolled differentiation of cellular therapies, making this a safer approach and one that can potentially be integrated into the clinical standard of care. NSC-EVs are easy to handle and retain high bioactivity over extended periods of time[2]. Our preclinical

studies demonstrated that human NSC-EVs did not induce any adverse effects and elicited a neuroprotective effect on non-immunosuppressed rats after repeated acute injections post-sTBI. Importantly, our results also demonstrated that NSC-EVs promotes endogenous NSC paracrine activity at the injury site in sTBI animals driving motor recovery, particularly, in male rats.

Evaluating sex differences in sTBI outcomes in human patients is highly challenging as injury outcome varies depending on the age and severity of the injury[3]. Previous reports suggest that females tend to have better functional outcomes than males in response to sTBI, which is mainly attributed to the expression of estrogen and progesterone[3]. Contrastingly, there is also evidence suggesting that female subjects suffer worse complications that persists longer than males[4]. Accumulating pre-clinical studies revealed differences in physiological responses such as inflammatory cytokine activation, vasculature disruption and neurodegeneration, and behavioral responses between males and females after sTBI[3]. These can be broadly attributed to the influence of sexual dimorphism on sTBI pathophysiology. Several reports have suggested sex-specific epigenetic regulation of genes, differential DNA methylation patterns, and alternative splicing of gene transcripts in the brain[5]. Despite an advanced understanding of cellular, synaptic, and circuit level differences in male and female brains[6], a fundamental understanding of how these differences influence functional outcomes after sTBI is currently lacking.

Sex-dependent neurogenesis and plasticity, as well as inflammatory responses are observed in sTBI[7-10]. Many studies have validated sex hormone linked differences in developing and mature brains. Elemental assessments of neuronal morphology such as the number of neural cells[11,12], fatty acid composition[13], and cell nucleus volume[14] indicated the likely involvement of androgen receptor in regulating sexually dimorphic brain development[15]. A separate study showed differential gene expression in male and female mouse brains prior to gonadal formation

suggesting that genetic factors may also contribute to brain sexual dimorphism[16]. Magnetic resonance imaging (MRI) studies demonstrated differences in cortical thickness, indicating that women possessed larger frontal and medial paralimbic cortices when compared to men, who instead exhibited the presence of a larger frontomedial cortex, the amygdala and hypothalamus[17,18]. Women also exhibited a significantly greater degree of interconnectedness (cross-modular), while male exhibit more localized and modular connectivity[19,20]. Learning patterns and social behaviors show dissimilarity due to these differences in network connectivity between males and females[5]. There is hence a multifaceted relationship between sexual dimorphism and neural function, which is likely to have a significant influence on sTBI outcomes.

Preclinical studies accounting for sex as a biological variable in sTBI investigations are generally lacking[21]. Results from our investigations on both male and female subjects in Chapter -2 suggest fundamental sex-differences in sTBI responses and therapeutic efficacy, which require detailed future investigations.

4.2 CS-based Brain-Mimetic Scaffolds to Regulate NSC Responses

Despite their initial promise as a cell and tissue replacement therapy, stem cell therapy now faces significant translational challenges due to low survival and engraftment of NSCs post-transplantation *in vivo*. In Chapter 3, we evaluate the design and modulation of CS sulfation as a cell-free approach to regulate endogenous NSC proliferation and maintenance, and to sustain the neuronal activity of differentiated neurons. This approach is based on increasing evidence of the dynamic roles played by CS in regulating NSC proliferation, self-renewal and cell lineage commitment within the central nervous system (CNS)[22]. Thus, the modulation of CS sulfation patterns can better inform the design and fabrication of multi-functional brain-mimetic scaffolds

that can be used to replace lost tissue and regulate endogenous NSC function after sTBI.

The functional integration of engineered 3D constructs as brain tissue replacements is heavily dependent on their ability to elicit native functionality and evoke immune tolerance. Both natural and synthetic polymers have been used to create 3D structures that resemble the brain microenvironment. These include natural polymers such as chitosan, collagen and hyaluronic acid, which are favored over synthetic polymers for their superior biocompatibility and biodegradability[23]. Alginate has been demonstrated to enhance NSC efficacy in a rat model of spinal cord injury by reducing the inflammatory responses as well as lesion size[24]. Hyaluronic acid hydrogels improved transplanted NSC survival and proliferation in mice[25]. Hydrogels composed of mixture of hyaluronan and heparin sulfate also demonstrated greater survival of NSCs in mice model of stroke [26]. On the other hand, synthetic polymers including those that belong to the polyester family, poly (anhydrides), and polyurethane poses advantages of easy processing and stable mechanical properties[27,28]. Plasma polymerized allylamine (ppAAm)-treated poly(d,l-lactic acid-*co*-glycolic acid) (PLGA) scaffold provided structural support for NSCs in stroke model of rats, which led to increased integration[29]. Polyethylene glycol scaffold were demonstrated to induce NSCs proliferation, migration, and differentiation in spinal cord injury model[30]. Despite these advances, current approaches are largely deficient in eliciting complex growth factor signaling and cellular homeostasis mediated by native ECM constituents such as sulfated CS-GAGs.

In Chapter-3, I designed and characterized the effects of sulfation-modulation of CS on hNSC maintenance, proliferation, and differentiation. I demonstrated that oversulfation of CS results in the significantly enhanced ability to promote NSC maintenance, migration, and aggregation, akin to the germinal niche in the brain. I also demonstrated that both mono- and

oversulfated CS microenvironments support neuronal activity and connectivity of neuronal networks, which reveals the potential for the design of more advanced ECM engineering approaches to regulate both NSC maintenance and neuronal differentiation. These *in vitro* studies reveal opportunities for detailed future investigations on the use of these constructs to modulate the injury microenvironment and regulate endogenous cellular responses after sTBI.

4.3 Conclusion

Cell-free therapy has gained popularity over the past decade due to its safe and efficacious treatment potential. To fully utilize the therapeutic benefits of these products, further understanding of specific disease/injury microenvironment as well as therapeutic mechanism of action is crucial. This dissertation contributes to bridging the knowledge gap in the use of cell-free therapies for treating sTBI. The non-invasive administration of NSC-EVs in experimental sTBI animals demonstrated sex-dependent neuroprotective effects via enhanced presentation of endogenous NSCs at the injury site leading to functional recovery. Sulfation-modified CS hydrogels provide a means of locally modulating the injury microenvironment to sustain NSC proliferation and promote neural network activity *in vitro*. In future, these synergistic approaches can be tailored in to prevent acute and chronic brain tissue loss and accelerate functional recovery after sTBI more effectively.

4.4 References

1 Lecky, F. *et al.* The Head Injury Transportation Straight to Neurosurgery (HITS-NS) randomised trial: a feasibility study. *Health Technol Assess* **20**, 1-198, doi:10.3310/hta20010 (2016).

2 Marban, E. The Secret Life of Exosomes: What Bees Can Teach Us About Next-Generation Therapeutics. *J Am Coll Cardiol* **71**, 193-200, doi:10.1016/j.jacc.2017.11.013 (2018).

3 Spani, C. B., Braun, D. J. & Van Eldik, L. J. Sex-related responses after traumatic brain injury: Considerations for preclinical modeling. *Front Neuroendocrinol* **50**, 52-66, doi:10.1016/j.yfrne.2018.03.006 (2018).

4 Farace, E. & Alves, W. M. Do women fare worse? A metaanalysis of gender differences in outcome after traumatic brain injury. *Neurosurg Focus* **8**, e6, doi:10.3171/foc.2000.8.1.152 (2000).

5 Choleris, E., Galea, L. A. M., Sohrabji, F. & Frick, K. M. Sex differences in the brain: Implications for behavioral and biomedical research. *Neurosci Biobehav Rev* **85**, 126-145, doi:10.1016/j.neubiorev.2017.07.005 (2018).

6 McCarthy, M. M., Arnold, A. P., Ball, G. F., Blaustein, J. D. & De Vries, G. J. Sex differences in the brain: the not so inconvenient truth. *J Neurosci* **32**, 2241-2247, doi:10.1523/JNEUROSCI.5372-11.2012 (2012).

7 Villapol, S., Loane, D. J. & Burns, M. P. Sexual dimorphism in the inflammatory response to traumatic brain injury. *Glia* **65**, 1423-1438, doi:10.1002/glia.23171 (2017).

8 Doran, S. J. *et al.* Sex Differences in Acute Neuroinflammation after Experimental Traumatic Brain Injury Are Mediated by Infiltrating Myeloid Cells. *J Neurotrauma* **36**, 1040-1053, doi:10.1089/neu.2018.6019 (2019).

9 Mottron, L. *et al.* Sex differences in brain plasticity: a new hypothesis for sex ratio bias in autism. *Mol Autism* **6**, 33, doi:10.1186/s13229-015-0024-1 (2015).

10 Yagi, S. & Galea, L. A. M. Sex differences in hippocampal cognition and neurogenesis. *Neuropsychopharmacology* **44**, 200-213, doi:10.1038/s41386-018-0208-4 (2019).

11 Forger, N. G. Control of cell number in the sexually dimorphic brain and spinal cord. *J Neuroendocrinol* **21**, 393-399, doi:10.1111/j.1365-2826.2009.01825.x (2009).

12 Ahmed, E. I. *et al.* Pubertal hormones modulate the addition of new cells to sexually dimorphic brain regions. *Nat Neurosci* **11**, 995-997, doi:10.1038/nn.2178 (2008).

13 Rodriguez-Navas, C., Morselli, E. & Clegg, D. J. Sexually dimorphic brain fatty acid composition in low and high fat diet-fed mice. *Mol Metab* **5**, 680-689, doi:10.1016/j.molmet.2016.06.014 (2016).

14 Swaab, D. F. & Fliers, E. A sexually dimorphic nucleus in the human brain. *Science* **228**, 1112-1115, doi:10.1126/science.3992248 (1985).

15 Shah, N. M. *et al.* Visualizing sexual dimorphism in the brain. *Neuron* **43**, 313-319, doi:10.1016/j.neuron.2004.07.008 (2004).

16 Dewing, P., Shi, T., Horvath, S. & Vilain, E. Sexually dimorphic gene expression in mouse brain precedes gonadal differentiation. *Brain Res Mol Brain Res* **118**, 82-90, doi:10.1016/s0169-328x(03)00339-5 (2003).

17 Goldstein, J. M. *et al.* Normal sexual dimorphism of the adult human brain assessed by in vivo magnetic resonance imaging. *Cereb Cortex* **11**, 490-497, doi:10.1093/cercor/11.6.490 (2001).

18 de Lima Xavier, L., Hanekamp, S. & Simonyan, K. Sexual Dimorphism Within Brain Regions Controlling Speech Production. *Front Neurosci* **13**, 795, doi:10.3389/fnins.2019.00795 (2019).

19 Cahill, L. Fundamental sex difference in human brain architecture. *Proc Natl Acad Sci U S A* **111**, 577-578, doi:10.1073/pnas.1320954111 (2014).

20 Ritchie, S. J. *et al.* Sex Differences in the Adult Human Brain: Evidence from 5216 UK Biobank Participants. *Cereb Cortex* **28**, 2959-2975, doi:10.1093/cercor/bhy109 (2018).

21 McCabe, J. T. & Tucker, L. B. Sex as a Biological Variable in Preclinical Modeling of Blast-Related Traumatic Brain Injury. *Front Neurol* **11**, 541050, doi:10.3389/fneur.2020.541050 (2020).

22 Purushothaman, A., Sugahara, K. & Faissner, A. Chondroitin sulfate "wobble motifs" modulate maintenance and differentiation of neural stem cells and their progeny. *J Biol Chem* **287**, 2935-2942, doi:10.1074/jbc.R111.298430 (2012).

23 Malafaya, P. B., Silva, G. A. & Reis, R. L. Natural-origin polymers as carriers and scaffolds for biomolecules and cell delivery in tissue engineering applications. *Adv Drug Deliv Rev* **59**, 207-233, doi:10.1016/j.addr.2007.03.012 (2007).

24 Hosseini, S. M., Sharafkhah, A., Koohi-Hosseinabadi, O. & Semsar-Kazerooni, M. Transplantation of Neural Stem Cells Cultured in Alginate Scaffold for Spinal Cord Injury in Rats. *Asian Spine J* **10**, 611-618, doi:10.4184/asj.2016.10.4.611 (2016).

25 Liang, Y., Walczak, P. & Bulte, J. W. The survival of engrafted neural stem cells within hyaluronic acid hydrogels. *Biomaterials* **34**, 5521-5529, doi:10.1016/j.biomaterials.2013.03.095 (2013).

26 Zhong, J. *et al.* Hydrogel matrix to support stem cell survival after brain transplantation in stroke. *Neurorehabil Neural Repair* **24**, 636-644, doi:10.1177/1545968310361958 (2010).

27 Gunatillake, P. A. & Adhikari, R. Biodegradable synthetic polymers for tissue engineering. *Eur Cell Mater* **5**, 1-16; discussion 16 (2003).

28 Bhang, S. H., Lim, J. S., Choi, C. Y., Kwon, Y. K. & Kim, B. S. The behavior of neural stem cells on biodegradable synthetic polymers. *J Biomater Sci Polym Ed* **18**, 223-239 (2007).

29 Bible, E. *et al.* The support of neural stem cells transplanted into stroke-induced brain cavities by PLGA particles. *Biomaterials* **30**, 2985-2994, doi:10.1016/j.biomaterials.2009.02.012 (2009).

30 Kong, X. B. *et al.* Polyethylene glycol as a promising synthetic material for repair of spinal cord injury. *Neural Regeneration Research* **12**, 1003-1008, doi:10.4103/1673-5374.208597 (2017).